Neutralizing human monoclonal antibodies that target the PcrV component of the Type III Secretion System of *Pseudomonas aeruginosa* act through distinct mechanisms

Jean-Mathieu Desveaux[1], Eric Faudry[1], Carlos Contreras-Martel[1], François Cretin[1], Leonardo Sebastian Dergan-Dylon[1], Axelle Amen[1,2], Isabelle Bally[1], Victor Tardivy-Casemajor[1], Fabien Chenavier[1], Delphine Fouquenet[3], Yvan Caspar[1,4], Ina Attrée*[1], Andréa Dessen*[1], Pascal Poignard*[1,5]

[1] Univ. Grenoble Alpes, CEA, CNRS, Institut de Biologie Structurale (IBS), F-38044 Grenoble, France

[2] Laboratoire d'Immunologie, CHU Grenoble Alpes, France

[3] Centre d'Étude des Pathologies Respiratoires INSERM U1100 UFR de Médecine de Tours, 10 Bd Tonnellé, 37032 Tours Cedex

[4] Laboratoire de Bactériologie-Hygiène Hospitalière, CHU Grenoble Alpes, France

[5] Laboratoire de Virologie, CHU Grenoble Alpes, France

* to whom correspondence should be addressed: ina.attree@ibs.fr, andrea.dessen@ibs.fr, pascal.poignard@ibs.fr

ABSTRACT

Pseudomonas aeruginosa is a major human opportunistic pathogen associated with a high incidence of multi-drug resistance. The antibody-based blockade of *P. aeruginosa* virulence factors represents a promising alternative strategy to mitigate its infectivity. In this study, we employed single B cell sorting to isolate, from cystic fibrosis patients, human monoclonal antibodies (mAbs) targeting proteins from the *P. aeruginosa* Type 3 Secretion System (T3SS) and characterized a panel of mAbs directed at PscF and PcrV. Among those, two mAbs, P5B3 and P3D6, that bind to the injectisome tip protein PcrV, exhibited T3SS blocking activity. We solved the crystal structure of the P3D6 Fab-PcrV complex, which revealed that the Ab binds to the C-terminal region of PcrV. Further, we compared the T3SS-blocking activity of three PcrV-targeting mAbs, including two from previous independent studies, using two distinct assays to evaluate pore formation and toxin injection. We conducted a mechanistic and structural analysis of their modes of action through modeling based on the known structure of a functional homolog, SipD from *Salmonella typhimurium*. The analysis suggests that anti-PcrV mAbs may act through different mechanisms, ranging from preventing PcrV oligomerization to disrupting PcrV's scaffolding function, thereby inhibiting the assembly and function of the translocon pore. Our findings provide additional evidence that T3SS-targeting Abs, some capable of inhibiting virulence, are elicited in *P. aeruginosa*-infected patients. The results offer deeper insights into PcrV recognition by mAbs and their associated mechanisms of action, helping to identify which Abs are more likely to be therapeutically useful based on their mode of action and potency. This paves the way for developing effective alternatives to traditional antibiotics in the fight against this resilient pathogen.

INTRODUCTION

The emergence of antimicrobial resistance is a major threat to human health. Among the microorganisms whose resistance rates have increased the most dramatically are ESKAPE pathogens (***E****nterococcus faecium,* ***S****taphylococcus aureus,* ***K****lebsiella pneumoniae,* ***A****cinetobacter baumannii,* ***P****seudomonas aeruginosa,* ***E****nterobacter spp*) for which novel antibacterial treatments are urgently needed. However, an antibiotic discovery hiatus that occurred during the last few decades severely heightened the resistance threat (Murray et al., 2022), underlining the importance of exploring alternative strategies such as host-targeting, bacteriophage, anti-virulence, and Ab-based therapies (De Melo et al., 2024; Kaufmann et al., 2018; Morrison, 2015).

Therapeutic mAbs have been successfully developed to fight viral infections ranging from Ebola to SARS-CoV-2 (Crowe, 2022; Levin et al., 2022; Mulangu et al., 2019). To date, however, only three therapeutic Abs have been marketed against bacteria, all of which target toxins. Other types of bacterial virulence factors could also serve as potential high importance targets for mAbs. Recent examples include the development of mAbs that target lipopolysaccharides, O-antigen, and outer membrane transporter proteins, notably in *Klebsiella pneumoniae* and *Mycobacterium tuberculosis* (Pennini et al., 2017; Rollenske et al., 2018; Watson et al., 2021). The advantages of targeting virulence factors through mAbs include notably a high specificity and the decreased likelihood of the emergence of resistance among bacteria (La Guidara et al., 2024). Additionally, the employment of mAb engineering platforms offers the potential for improved efficacy through modifications such as half-life extension and alterations of Fc effector functions (Morrison, 2015; Vacca et al., 2022). Finally, strategies such as the use of mAb cocktails targeting different specificities and the combination with traditional antibiotics further expand the range of Ab-based treatment options (Duan et al., 2021; Morrison, 2015; Tabor et al., 2018).

Pseudomonas aeruginosa is a major nosocomial pathogen and the leading cause of acute pneumonia and chronic lung infections, particularly in ventilator-assisted and cystic fibrosis (CF) patients. Infections with *P. aeruginosa* ultimately lead to loss of lung function and death in CF patients. Worldwide, *P. aeruginosa* is responsible for more than 300,000 deaths associated or attributed to resistance each year. The natural resistance of *P. aeruginosa* to a broad range of antibiotics, its ability

to grow as biofilms, as well as its widespread presence in hospital settings (Horcajada et al., 2019; Murray et al., 2022), have called for urgent efforts towards the development of new therapeutic agents. Aggressive acute infections by *P. aeruginosa* are highly dependent on its Type III Secretion System (T3SS), a needle-like, multi-component secretion machinery located on the cell surface and that transports effectors from the bacterial cytoplasm directly into the host cell cytosol (Goure et al., 2004; Hauser, 2009; Quinaud et al., 2007, 2005). It is of note that in other human pathogens such as *Yersinia pestis*, *Salmonella typhi*, *Shigella dysenteriae* and *Escherichia coli* the T3SS also plays a key role in virulence, participating in the causation of diseases such as plague, typhoid fever, and bacillary dysentery, respectively (Coburn et al., 2007; Diepold and Wagner, 2014; Hu et al., 2017; Serapio-Palacios and Finlay, 2020).

A key component of the T3SS is the injectisome, membrane-embedded protein rings extended by a hollow needle, composed of the PscF protein that protrudes outwards from the bacterial surface. Injectisome-dependent toxin delivery, which occurs upon contact with the eukaryotic target cell, also requires formation of the 'translocon', a complex of three proteins that are exported through the interior of the polymerized needle, assemble at its tip and form a pore in the eukaryotic cell membrane, an essential step for effector injection (Mueller et al., 2008). The translocon is composed of two hydrophobic proteins (PopB and PopD in *P. aeruginosa*), as well as a hydrophilic partner - PcrV, or the V antigen- in *P. aeruginosa* (Matteï et al., 2011). PopB and PopD have been shown to act as *bona fide* pore-forming toxins (Schoehn et al., 2003; Faudry et al., 2006; Montagner et al., 2011) that, upon membrane disruption, can trigger the manipulation of host processes including histone dephosphorylation and mitochondrial network disruption (Dortet et al., 2018). PcrV, on the other hand, oligomerizes at the tip of the T3SS needle and aids PopB and PopD in their membrane disruption process (Gébus et al., 2009; Goure et al., 2005; Guo and Galán, 2021; Matteï et al., 2011). Crystal structures of monomeric homologs of PcrV (LcrV, SipD, BipD) have shown that they fold into an elongated coiled-coil buttressed by an α-helical hairpin at the N-terminus and an α/β carboxy-terminal region (Derewenda, 2011; Erskine et al., 2006; Lunelli et al., 2011). Notably, the cryo-EM structure of a needle filament complex composed of PrgI (needle protein) with SipD (tip protein) at its extremity confirmed that the latter forms a pentamer where the first

124 and fifth subunits are separated by a gap, thus generating a heterogeneous assembly
125 (Guo and Galán, 2021). This arrangement could be similar in numerous T3SS systems
126 (Habenstein et al., 2019).

127 Given the importance of the T3SS for *P. aeruginosa* infection, components such
128 as PcrV and PscF have been explored as targets for the development of therapeutic
129 Abs and inhibitory small molecules, respectively (Berube et al., 2017; Bowlin et al.,
130 2014). Animal models have shown that blocking the T3SS, particularly the function of
131 PcrV, can successfully diminish tissue damage due to *P. aeruginosa* infection (Frank
132 et al., 2002; Imamura et al., 2007). Moreover, in ventilated patients, pegylated Fabs
133 that target PcrV (KB001-A) were shown to successfully reduce the incidence of
134 pneumonia, which is consistent with the role of T3SS in the acute phase of infection
135 (Jain et al., 2018; Roy-Burman et al., 2001). However, this treatment did not benefit
136 chronically colonized CF patients in terms of antibiotic needs (François et al., 2012;
137 Jain et al., 2018; Yaeger et al., 2021). In addition, the bispecific MEDI3902 mAb
138 targeting both PcrV and the Psl exopolysaccharide successfully protected against *P.*
139 *aeruginosa* infection in animal models but was discontinued in phase II clinical trials
140 (Chastre et al., 2022; DiGiandomenico et al., 2014). Nevertheless, PcrV remains an
141 attractive target, motivating the search for potentially more effective Abs (Simonis et
142 al., 2023).

143 Here, we sorted specific single memory B cells from peripheral blood
144 mononuclear cells (PBMCs) of cystic fibrosis patients to identify mAbs against PcrV
145 and PscF with potential T3SS-inhibiting activity. Two anti-PcrV mAbs (P5B3 and P3D6)
146 showed inhibition of the injection of the T3SS effector ExoS into epithelial cells, with
147 mAb P5B3 displaying blocking activity against five major PcrV variants representing
148 more than 80% of clinical isolates sequenced to date. We obtained the crystal structure
149 of a P3D6 Fab-PcrV complex and further compared the mechanisms of actions of
150 different anti-PcrV mAbs targeting various epitopes, including one mAb from a recent
151 publication (Simonis et al., 2023). These structure-based analyses of the mechanisms
152 of action of the different mAbs provide valuable insights for the development of
153 improved antipseudomonal treatments and preventive approaches.

154

155

156 **RESULTS**

157

158 **Selection of donors exhibiting T3SS-inhibiting circulating IgG responses**

159 Our approach was based on single cell sorting of recombinant PcrV and PscF
160 specific memory B cells from human donor peripheral blood mononuclear cells
161 (PBMCs). To identify donors with anti-PcrV and -PscF mAbs with T3SS-inhibitory
162 activity, we first evaluated in ELISA the reactivity of sera from a cohort of CF patients
163 that were chronically colonized with *P. aeruginosa* against recombinant PcrV and PscF
164 before testing them in functional assays (Figure 1A). Among the 34 sera tested, donors
165 16 and 25 exhibited the strongest reactivity for both proteins (Figure 1B).

166 To assess the capacity of serum-purified IgGs to block T3SS effector
167 translocation, we used a previously developed cellular model that is based on the
168 T3SS-dependent translocation of the ExoS effector fused to β-lactamase, ExoS-Bla
169 (Verove et al., 2012). Briefly, epithelial cells were exposed to *P. aeruginosa* CHA∆*exoS*
170 expressing the ExoS-Bla reporter in the presence of patients' polyclonal purified IgGs.
171 ExoS-Bla translocation was measured by monitoring fluorescence of the β-lactamase
172 FRET-competent substrate CCF2-AM, and expressed as normalized reporter injection.
173 Polyclonal IgGs from donors 16 and 25 showed a potent ExoS-Bla translocation
174 blocking activity with an almost complete inhibition of injection at 160 µg/mL (Figure
175 1C). To investigate whether the observed activity was driven by anti-PcrV and/or anti-
176 PscF specific IgGs, we absorbed specific Abs on beads coated with recombinant PcrV
177 or PscF to obtain polyclonal IgG samples depleted of the corresponding specific IgGs
178 (Figure 1D, top). The T3SS blocking activity of depleted polyclonal IgGs was then
179 evaluated using the same method as above (Figure 1D, bottom). The results showed
180 a decrease in inhibitory activity when anti-PcrV Abs were depleted from donor 25's
181 IgGs and when anti-PscF Abs were depleted from donor 16's IgGs, suggesting the
182 presence of inhibitory Abs against the respective proteins. Additionally, the findings
183 demonstrated that our recombinant antigen baits could effectively bind T3SS-inhibitory
184 Abs and could therefore be used to isolate memory B cells producing the
185 corresponding IgGs.

186

187 **Isolation of PcrV and PscF mAbs using a single cell direct sorting approach**

188 To isolate mAbs specific to PcrV and PscF, PBMCs were purified from whole
189 blood from the two selected donors. Next, using single cell sorting, IgG positive
190 memory B cells were isolated based on their ability to recognize either PscF or PcrV
191 (Figure 2A) and seeded at the frequency of one cell per well. Variable heavy and light
192 chain gene sequences were retrieved from isolated B cells leading to the production of
193 a total of 66 recombinant mAbs (53 and 13 putative anti-PscF and anti-PcrV,
194 respectively). The specific binding capacities of 10 anti-PscF and 4 anti-PcrV mAbs
195 were confirmed by ELISA against the corresponding recombinant proteins. EC_{50}
196 values calculated from ELISA data showed variable apparent affinities ranging from
197 ~50 µg/mL to 0.02 µg/mL (Figure 2B). Isolated mAbs originated from a variety of
198 variable gene germline families, as determined using the international immunogenetics
199 information system (IMGT) database alignments, and did not present any notable
200 features in term of mutation rates or HCDR3 length (Supplementary Table 1), with no
201 particular enrichment noted.

202 The ability of ELISA-confirmed anti-PscF and anti-PcrV mAbs to block T3SS-
203 mediated activity at a concentration of 100 µg/mL was subsequently evaluated using
204 the ExoS-Bla reporter system. No significant reduction in ExoS-Bla injection was
205 observed for any of the anti-PscF mAbs tested. However, two out of four anti-PcrV
206 mAbs, P5B3 and P3D6, significantly reduced ExoS-Bla injection, with P3D6 displaying
207 significantly stronger efficacy (Figure 2B).

208 To map the epitopes of the isolated mAbs, we next performed competition
209 ELISAs (Supplementary Table 2). Antibodies directed at PscF grouped into three
210 clusters, with P1D8 and P5G10 mAbs competing only against themselves. Similarly,
211 anti-PcrV mAbs also grouped into three clusters, with the two anti-PcrV mAbs
212 exhibiting T3SS inhibitory activity, P5B3 and P3D6, seemingly targeting overlapping
213 epitopes. Precise affinities of both mAbs were measured using biolayer interferometry
214 (BLI), revealing subnanomolar K_D values (Supplementary Table 3). Notably, P3D6
215 exhibited approximately 30-fold lower affinity compared to P3B3, despite
216 demonstrating greater efficacy in the inhibitory assay.

217

218 **P5B3 inhibits T3SS-dependent toxin injection by recognizing a highly conserved**
219 **epitope of PcrV**

220 Polymorphism in PcrV protein sequences was reported among *P. aeruginosa*
221 clinical isolates and should be considered in the development of therapeutic human
222 monoclonal Abs targeting PcrV (Figure 3A) (Tabor et al., 2018). To determine whether
223 the blocking activity of mAbs P5B3 and P3D6 was impacted by the PcrV sequence,
224 the reporter ExoS-Bla was introduced into a strain that lacked isogenic PcrV (Δ*pcrV*)
225 and synthetized the five most prevalent PcrV variants found in over 80% of clinical
226 isolates (Tabor et al., 2018). Monoclonal Ab P5B3 showed statistically significant T3SS
227 blocking activity towards all variants (Figure 3B) with estimated IC_{50} values of 100
228 μg/ml for variants 1, 2, 3, 4 and 400 μg/ml for variant 5 (Supplementary Figure 1). In
229 contrast, mAb P3D6 had no effect on variants 2, 3, 4 and 5, but strongly inhibited
230 variant 1 (Figure 3B) with an estimated IC_{50} of 3.7 μg/ml (Supplementary Figure 1),
231 indicating that the epitope recognized by P3D6 differs between PcrV variants.

232

233 **Anti-PcrV mAbs block translocon pore assembly**

234 It has been suggested that PcrV scaffolds the assembly of the PopB/PopD
235 translocon within host membranes by interacting with the PopD component of the pore
236 (Goure et al., 2004; Kundracik et al., 2022, 2022; Matteï et al., 2011). Furthermore,
237 polyclonal Abs raised against PcrV have been shown to inhibit the assembly of the
238 translocon in target membranes (Goure et al., 2005).

239 To investigate the mechanistic details of the inhibitory activity of mAbs P3D6
240 and P5B3, we used a *P. aeruginosa* strain deprived of all three T3SS effectors, ExoS,
241 ExoT and ExoY. This strain, named PAO1Δ3Tox (Cisz et al., 2008) harbors PcrV
242 variant 1 and provokes toxin-independent macrophage pyroptosis upon membrane
243 insertion of the PopB/PopD translocation pore (Dacheux et al., 2001). Death of J774
244 macrophages was monitored during 4h post-infection by measuring an increase in
245 propidium iodide fluorescence due to DNA binding to the nuclei of dead cells. Both
246 mAbs significantly reduced the cytotoxicity induced by PAO1Δ3Tox by 28% and 73%,
247 respectively (Figure 4A). Monoclonal Ab P3D6 exhibited a dose-response inhibition
248 with an estimated IC_{50} of 11.8 μg/mL (Figure 4B), while P5B3 did not exhibit a

249 significant dose-response effect at concentrations below 100 µg/mL (Figure 4C).
250 Overall, these results indicate that the binding of both mAbs to PcrV reduces the
251 formation of the translocation pore in target cell membranes, with P3D6 exhibiting more
252 potent activity.

253

254 **Crystal structure of PcrV* bound to Fab P3D6**

255 In order to identify the PcrV epitopes recognized by the two mAbs, we generated
256 a plasmid encoding a form of PcrV (PcrV*) amenable to crystallization (Tabor et al.,
257 2018) as well as Fab fragments from both P3D6 and P5B3 mAbs. PcrV* was
258 expressed in *E. coli* while both Fabs were expressed in HEK293F cells. Individual
259 proteins were purified by affinity and size-exclusion chromatographies. PcrV* was
260 incubated with either Fab fragment and samples were co-purified using size exclusion
261 chromatography. Despite the fact that both PcrV*-Fab P3D6 and PcrV*-Fab P5B3
262 complexes co-eluted in gel filtration, only the PcrV*-Fab P3D6 complex subsequently
263 generated diffracting crystals. Data were collected at the ESRF synchrotron in
264 Grenoble and the structure was solved by molecular replacement using Phaser
265 (McCoy et al., 2007). Iterative manual model building and model improvement led to
266 the structure whose statistics for data collection and refinement are presented in
267 Supplementary Table 4.

268 PcrV* is composed of six helices interwoven by loop regions. α-helices 1, 4 and
269 6 are the major secondary structure elements in PcrV*, while helices 2, 3 and 5 are 1-
270 or 2-turn helices. Most of the contacts formed between PcrV* and Fab P3D6 involve
271 Helix 6 and the loop preceding it (Figures 5A, 5B) and implicate a binding platform
272 made by both LC and HC from Fab P3D6. From the PcrV side, the interaction region
273 is highly polar, being formed by the side chains of Lys208, Gln217, Glu220, Lys222,
274 Ser225, Asp 226, Tyr 228, Glu231, Asn234, Thr243, Asp246 and Arg247. The
275 substitution of Ser225 in PcrV variant V1 by Lys or Arg in variants V2 to V5 is consistent
276 with P3D6 being inefficient on strains harboring these four variants.

277 In order to understand the protective role of mAb P3D6 in the context of the
278 PcrV pentameric oligomer located at the tip of the PscF needle, we generated a model
279 using the cryo-EM structure of the SipD pentamer (Guo and Galán, 2021) and aligned
280 our co-crystal structure onto this model (Figures 5C, 5D).This analysis revealed that

281 Fab P3D6 can successfully bind to one PcrV monomer (dark red and orange in Figure
282 5, respectively), but would be unable to bind to a pre-formed PcrV pentamer due to the
283 generation of clashes with neighboring subunits of the oligomeric form (Figure 5; the
284 structure of the Fab can be seen overlaid with that of the pentamer subunits).

285

286 **DISCUSSION**

287 We generated a panel of anti-PscF and -PcrV human mAbs through specific
288 memory B cell sorting from selected individuals. Although adsorption experiments with
289 recombinant PscF suggested the presence of anti-PscF Abs with T3SS inhibitory
290 activity in the donor from whom they were isolated, none of the isolated mAbs exhibited
291 this activity. Competition mapping showed that the anti-PscF mAbs targeted three
292 distinct regions of PscF, none of which seemingly involved in inhibitory activity. Further
293 epitope mapping would be necessary to gain deeper insight; however, in the absence
294 of a PscF structure, this remains challenging. Isolating a greater number of mAbs from
295 a selected donor with strong anti-PscF inhibitory activity would certainly increase the
296 likelihood of identifying one with T3SS-inhibiting properties.

297 Of the four anti-PcrV mAbs isolated, two exhibited T3SS inhibitory capacity.
298 Their mechanism of action could potentially involve (i) prevention of effector secretion
299 by acting as a cap for PcrV; (ii) prevention of effector translocation towards the host
300 cell by disruption of the PcrV-PopB/PopD interaction; or (iii) prevention of
301 oligomerization of PcrV itself (Gébus et al., 2009; Sawa et al., 2019). Here, we
302 measured the ability of the inhibiting anti-PcrV mAbs we isolated to block PopB/PopD
303 pore formation and toxin injection, and carried out a mechanistic and structural analysis
304 of their activity, in parallel with other mAbs targeting PcrV.

305 We set out to investigate and compare the mechanism of action of several anti-
306 PcrV mAbs: P3D6 mAb and P5B3 (this work), 30-B8 (Simonis et al., 2023), as well as
307 a previously reported humanized, bivalent PcrV-Psl mAb (DiGiandomenico et al.,
308 2014). In order to do so, we produced mAb 30-B8 and subsequently purchased mAb
309 MEDI3902 from MedChem. The P3D6, P5B3, 30-B8 and MEDI3902 mAbs were
310 notably compared by employing two assays capable of detecting T3SS inhibition, each
311 with a different readout: injection of the ExoS-Bla reporter into epithelial cells and
312 cytotoxicity measurements in macrophages as a read-out for translocon assembly. In

313 addition, we performed structural analyses on three of the mAb-PcrV complexes, from
314 the viewpoints of recognition of both monomeric and pentameric forms of PcrV.

315 Both MEDI3902 and 30-B8 mAbs potently inhibited the injection of ExoS-Bla
316 into target cells, with IC_{50} values of 117 ng/ml and 21.3 ng/ml, respectively (Figure 6A).
317 Monoclonal Abs isolated in this study also inhibited toxin injection, although
318 significantly less potently, with IC_{50} values of 3.65 µg/mL for P3D6, and around 100
319 µg/mL for P5B3. Monoclonal Ab MEDI3902 had previously been shown to bind to
320 different PcrV variants (Tabor et al., 2018) and here we confirmed that mAb 30-B8 was
321 similarly efficient at inhibiting toxin injection by strains carrying five different PcrV
322 variants (Simonis et al., 2023) (Supplementary Figure 2). Monoclonal Ab P5B3 was
323 also able to inhibit all variants, but only at high concentrations, while P3D6 was only
324 active against variant V1. Therefore, P5B3 appears to recognize a highly conserved
325 epitope whereas P3D6 seems to bind an overlapping epitope that includes the variable
326 Ser225, as suggested by the ELISA mapping competition and structural data, but does
327 so in a more effective manner.

328 In the macrophage cytotoxicity assay, translocon assembly was inhibited by
329 mAbs 30-B8 (IC_{50} of 45.2 ng/ml) and P3D6 (IC_{50} of 11.8 µg/mL), while P5B3 and
330 MEDI3902 did not exhibit significant dose-response inhibition. Together, these results
331 suggest that the T3SS-inhibiting activity of these anti-PcrV Abs may occur through
332 distinct mechanisms.

333 In order to understand the differences in potency and potentially in mechanisms
334 of action at a structural level, we compared the Fab-PcrV interaction regions for the
335 P3D6, 30-B8 and MEDI3902 Fabs. Monomeric PcrV is an elongated, dumbbell-shaped
336 molecule, and the chimeric form used in this study displays the same characteristics
337 (Figure 5A). Fab MEDI3902 binds to one of the extremities of monomeric PcrV,
338 extending in the longitudinal axis of the molecule (Figure 6B, top). This mode of binding
339 is distinct from that of 30-B8 and P3D6 Fabs, both of which recognize the C-terminal
340 region of PcrV (Figure 6B, middle) (Simonis et al., 2023). Therefore, the binding region
341 of 30-B8 and P3D6 does not, by itself, appear to explain the significant difference in
342 potency between the two mAbs. Moreover, a difference in affinity does not account for
343 the difference in potency either, as both mAbs bind to recombinant monomeric PcrV
344 with comparable apparent affinities of around 30 ng/ml (our data and Simonis et al.,
345 2023).

346 In order to perform this comparative analysis in the context of a PcrV oligomer,
347 we employed the model of the PcrV pentamer generated as described above, which
348 was based on the cryo-EM structure of SipD from *S. typhimurium* (Guo and Galán,
349 2021). According to this analysis, the only Fab that is able to bind to all PcrV protomers
350 in the pentamer without generating clashes with either PcrV or other Fabs is 30-B8
351 (Figure 6). In the case of MEDI3902, the Fab can bind the oligomer, but only with a 1:5
352 stoichiometry, due to possibility of clashes between Fabs. Finally, P3D6 is unable to
353 bind to a pre-formed pentamer, and can only recognize a PcrV protomer in its
354 monomeric form.

355 This structural analysis suggests different potential mechanisms of action. For
356 P3D6, the inability to bind to the pentamer points towards a mechanism involving
357 inhibition of oligomerization. Indeed, the analysis shows that binding of P3D6 to a
358 single PcrV monomer prevents the association of additional PcrV protomers through
359 Fab-protomer direct clashes. A similar mechanism of action may be suggested for
360 MEDI3902, as Fab-bound PcrV protomers cannot oligomerize, in this case due to
361 clashes between the Fabs themselves (Fig. 6). However, the fact that MEDI3902 does
362 not appear to prevent translocon insertion suggests that such a mechanism is unlikely
363 for this mAb as PcrV oligomerisation is required at the tip of the needle for translocon
364 assembly. In contrast to P3D6, MEDI3902 can bind the oligomerized PcrV pentamer
365 (with a stoichiometry of one) and its mechanism of action may thus be related to this
366 ability. Our results suggest that when MEDI3902 is bound to the PcrV oligomer, the
367 formation of the pore is not efficiently blocked while toxin injection is strongly inhibited
368 (Fig. 6). Therefore, the presence of one MEDI3902 Ab molecule at the tip of the needle
369 does not appear to efficiently prevent either the secretion of the translocator proteins
370 PopB/PopD through the needle, nor the interactions between PcrV and PopB/PopD,
371 which have been described as required for pore formation (Kundracik et al., 2022).
372 However, the MEDI3902 Ab molecule, seems to interfere with further interactions
373 between PcrV and the PopB/PopB complex, or with the sensing by PcrV of the host
374 cell, both of which are needed for toxin injection (Lee et al., 2010).

375 Lastly, 30-B8, which can bind the formed pentamer with a stoichiometry of five,
376 appears to be the most effective at blocking both pore formation and toxin injection.
377 The fact that the PcrV-bound 30-B8 Ab probably projects towards the cell membrane,

378 associated with its ability to bind to the PcrV pentamer at full occupancy, may result in
379 remarkable efficacy in blocking the interactions between PcrV and PopB/PopD.

380 In conclusion, here we show that patients with chronic infection with *P.*
381 *aeruginosa* can elicit anti-PscF and anti-PcrV mAbs that recognize different regions
382 within these proteins. Anti-PcrV Abs can act as T3SS inhibitors through different
383 mechanisms, with some exhibiting significantly greater efficacy than others. The
384 strategy employed here, involving the analysis of structural and functional data on anti-
385 T3SS mAbs should open new avenues towards deciphering the mechanism of T3SS
386 toxin translocation and enable the isolation of more effective mAbs targeting a broad
387 range of clinical strains.

388

389 **MATERIALS and METHODS**

390 **Clinical sample collection**

391 The study was approved by the French ethics committee (ID-RCB 2020-
392 A00311-38) and was carried out according to the Declaration of Helsinki, Good Clinical
393 Practice (GCP) guidelines and current French regulations. Written consent for
394 participation was not required for this study. The first phase was a non-interventional
395 study involving data and samples from human participants conducted according to
396 Reference Methodology No. 004 issued by French authorities (Commission Nationale
397 de l'Informatique et des Libertés). Screening and functional assays were performed on
398 human sera previously collected at Grenoble Alpes University Hospital (France), from
399 CF patients chronically infected with *P. aeruginosa*. Participants were all informed and
400 did not object to this phase of the study. Inclusion criteria for the second phase of the
401 study were: patients with positive screening during phase one, ≥ 18 years old, ≥32 Kg,
402 with a programmed blood sampling at Grenoble Alpes University Hospital and not
403 being opposed to the second phase of the project. Whole blood was then collected
404 using BD Vacutainer® EDTA tubes (Becton Dickinson) and PBMCs were purified by
405 density gradient centrifugation using Lymphoprep (Eurobio scientific) following
406 manufacturing guidelines. Cells were then stored in liquid nitrogen until further use.

407

408 **Bacterial strains, genetic manipulations and growth conditions**

409 *P. aeruginosa* strains used in this study are listed in Supplementary Table 5.
410 Strains were cultured in LB media at 37 °C. For infection experiments, bacteria were
411 grown until the measured optical density at 600 nm (OD_{600nm}) of 1. The genes
412 encoding the most common variants of PcrV were cloned into the *Pseudomonas*
413 replicative vector derived from pUCP21 (West et al., 1994) containing the P*pcrG*
414 promoter driving the *pcrGVHpopDB* operon expression (West et al., 1994). The
415 plasmids, kindly provided by Simona Barzu (Sanofi Pasteur, Lyon), were
416 transformed into the *P. aeruginosa* strain CHA lacking *pcrV* (Goure et al., 2004).
417

418 **Expression and purification of full length PcrV and PcrV***

419 Expression of full-length PcrV from strain PAO1, cloned into a pET15b vector,
420 was performed in *E. coli* BL21(DE3) as previously described, with small modifications
421 (Nanao et al., 2003). Expression was induced with 1mM of Isopropyl β-D-1-
422 thiogalactopyranoside (IPTG) at OD_{600} = 0.8 AU and cells were then grown overnight
423 at 20°C with shaking at 250 rpm. Cells were harvested by centrifugation and lysed by
424 passing through a French Press 3 times at 25 Kpsi in lysis Buffer (50 mM Tris pH8,
425 200 mM NaCl, 20 mM Imidazole) supplemented with a protein inhibitor cocktail tablet
426 (ROCHE). The supernatant was cleared by centrifugation at 18,000 rpm and
427 subsequently loaded onto Ni-IDA resin (Macherey-Nagel). The resin was washed with
428 lysis buffer and the sample was eluted with lysis buffer supplemented with 100 mM
429 imidazole. Fractions containing the sample were pooled and applied to a size-
430 exclusion chromatography column (Superdex 200 HiLoad 16/600) pre-equilibrated in
431 SEC buffer (20mM Tris pH 8, 150 mM NaCl, 1 mM EDTA). A chimeric form of PcrV
432 (PcrV*) consisting of amino acids 1-17 fused to 136-249, was constructed based on a
433 construct made by Tabor et al. (2018) and employed for crystallization purposes. The
434 purification protocol was the same as above, the only difference being that 250 mM
435 imidazole was employed to elute the sample from the Ni resin.

436

437 **Expression and purification of PscF**

438 Expression of PscF from strain PAO1 was performed in *E. coli* BL21(DE3)
439 grown in Terrific Broth. Expression was induced with 1 mM Isopropyl β-D-1-
440 thiogalactopyranoside (IPTG) at OD_{600} = 0.6 AU and cells were then grown for an

441 additional 3 hours at 37 °C with shaking at 250 rpm. Cells were harvested by
442 centrifugation and lysed by passing through a French Press 3 times at 25 kpsi in lysis
443 buffer (50 mM Tris pH 8, 200 mM NaCl, 20 mM Imidazole, 2 % glycerol) supplemented
444 with a protein inhibitor cocktail tablet (Roche). The supernatant was cleared by
445 centrifugation at 18,000 rpm and applied to a Ni-IDA resin (Macherey-Nagel). The resin
446 was washed with lysis buffer and the protein was eluted with lysis buffer supplemented
447 with 250 mM imidazole. Fractions were then buffer exchanged in an Amicon Ultra 10
448 kDa cutoff concentrator against a buffer exempt of imidazole (50 mM Tris pH 8, 200
449 mM NaCl, 2 % glycerol).

450

451 **ELISA assays**

452 For direct ELISA assays, serial dilutions of sera or mAbs were transferred in
453 antigen-adsorbed wells of 96-well plates. Antigen binding was detected by an alkaline
454 phosphatase-conjugated goat anti-human immunoglobulin G (IgG) F(ab′)2 Ab
455 (Jackson Immuno). For competition ELISA, serial dilution of competitor mAbs were
456 transferred in antigen-adsorbed wells. Following an incubation of 30 min, biotinylated
457 mAbs were added to the wells at a concentration corresponding to the EC_{70} (Effective
458 concentration 70). Biotinylated mAbs were detected using alkaline phosphatase
459 conjugated streptavidin. Polyclonal Abs raised in rabbits against PscF and PcrV
460 (Goure et al., 2004) were used as positive controls.

461

462 **Sorting of specific memory B cells**

463 Briefly, PBMCs were stained for 30 min at 4ºC in the dark, using Facs-Buffer
464 (PBS-1X 0,5 % BSA , 2mM EDTA) with Live Dead staining (Thermo L34957), Anti-
465 human CD3-Vio-Blue (Miltenyi 130-114-519), Anti-human CD20 Pe-Vio707 (Miltenyi
466 130-111-345), Anti-human CD19 Pe-Vio707 (Miltenyi 130-113-649), Anti-human IgM
467 PE (Miltenyi 130-093-075), Anti-human IgA PE (Miltenyi 130-113-476), Anti-human
468 IgD PE (Miltenyi 130-110-643), Anti-human CD27 APC (Miltenyi 130-108-336), in the
469 presence of recombinant biotinylated His-PcrV-Avitag coupled with streptavidin
470 BUV737 (BD 612775) or streptavidin Vio-515 (Miltenyi 103-107-459), and
471 recombinant biotinylated His-PscF-Avitag coupled with streptavidin BUV496 (BD

472 612961) or streptavidin BV605 (Biolegend 405229). After washing, the cells were
473 resuspended in Facs-Buffer and PscF or PcrV positive B cells are sorted and clonally
474 seeded in 96 plates containing lysis buffer using BD FACSAria Fusion cytometer (BD
475 Biosciences).

476

477 **Isolation and production of mAbs**

478 Sequences coding for variable regions of both heavy and light (κ and λ) chains
479 were isolated by reverse transcription on total mRNA followed by a multiplex nested
480 PCR using a set of primers covering the diversity of V-region diversity. V-regions family
481 was attributed after sequencing of amplicons and alignment in the IMGT database
482 (https://imgt.org). An additional round of PCR using primers specific to the identified
483 family was performed followed by the cloning of V-regions genes in corresponding
484 vectors containing IgG1H, IgGκ and IgGλ constant regions. MAbs were recovered by
485 transient transfection in HEK293F cells (ThermoFisher scientific) and purification by
486 affinity chromatography using Protein A Sepharose (Sigma). Regarding 30-B8, the
487 sequences coding for the variable regions of heavy and light chains were synthesized
488 by Eurofins according to the sequence published by Simonis and coworkers (Simonis
489 et al., 2023). Cloning and production were performed as described above.

490

491 **P3D6 and P5B3 Fab production**

492 Sequences coding for Fab fragments were obtained by inserting stop codons
493 on genes corresponding to heavy chains of the mAbs by PCR using site directed
494 mutagenesis (Quickchange II, Agilent) according to manufacturer's instructions.
495 Mutated heavy and corresponding light chain genes were cloned into appropriate
496 expression plasmids for eukaryotic cell expression and were co-transfected at a 2:1
497 ration into FreeStyle 293-F cells (ThermoFisher). Fabs were purified using
498 KappaSelect affinity chromatography (Cytiva).

499

500 **Cellular tests for T3SS activity**

501 *ExoS-Bla translocation*

502 The T3SS-dependent toxin injection into epithelial A549 cells was measured
503 using the reporter system based on Bla/CCF2 enzyme/substrate combination
504 (Charpentier and Oswald, 2004) previously described for *P. aeruginosa* (Verove et
505 al., 2012). *P. aeruginosa* strain CHAΔ*exoS* carring ExoS-Bla fusion on the
506 chromosome was used to infect A549 cells at the multiplicity of infection (MOI) of 5.
507 The level of injected ExoS-β-lactamase was measured using CCF2 substrate, as
508 described previously (Verove et al., 2012). All values were normalized using non-
509 infected cells and cells infected in the absence of Abs as references.
510
511 *Pore formation / propidium iodide incorporation into macrophages*
512 To assess the formation of a T3SS translocation pore, macrophages were
513 infected with a *P. aeruginosa* strain PAO1Δ3Tox devoid of three exotoxins (Cisz et al.,
514 2008). Two days before the experiment, J774 cells were seeded in a 96-well plate
515 (Greiner, 655090) at a density of 100 000 cells per well in DMEM supplemented with
516 10% FCS. The day before the experiment, the strain was grown overnight in LB
517 medium. The next day, bacteria were sub-cultures in fresh LB media until an OD_{600nm}
518 of 1 and the macrophages were washed two times with PBS before addition of 65 µL
519 of DMEM 10% FCS containing 2 µg/mL of Propidium Iodide. Antibodies diluted in
520 DMEM, 10% FCS (25 µL) were then added followed by 10 µL of bacteria diluted in
521 DMEM 10% FCS to give a MOI of 5. Propidium iodide fluorescence was recorded in a
522 Fluoroskan fluorimeter every 10 minutes. The data of each fluorescence kinetics of the
523 triplicates were processed in R Studio to calculate the Area Under the Curve, as
524 described before (Ngo et al., 2019). This metrics was then normalized using non-
525 infected cells and cells infected in the absence of Abs as references.
526
527 **Data processing and analysis**
528 Data from independent cell experiments were pooled and analyzed in R Studio
529 by one-way ANOVA followed by paired t-test or Kuskal-Wallis followed by the Dunn
530 test. Dose-response fitting was performed using the drc package and logistic models.
531
532 **Bio-layer interferometry**
533 BLI experiments were performed on an OctetRED96e from Satorius/FortéBio
534 (former Pall/FortéBio) and were recorded with software provided by the manufacturer

535 (Data Acquisition v11.1). All protein samples were diluted in analysis buffer (1X PBS
536 pH 7.4, 0.02% Tween-20). 10 mM glycine pH 2.0 was used as regeneration buffer.
537 Commercial SA or SAX (streptavidin) biosensors (Pall/FortéBio) were used to capture
538 biotinylated PcrV. Kinetic analyses were performed in black 96-well plates (Nunc F96
539 MicroWell, Thermo Fisher Scientific) at 25°C with agitation at 1000 rpm. After
540 incubation and equilibration of biosensors in analysis buffer, PcrV samples were
541 applied at a concentration of 2.5 mg/ml by dipping biosensors until reaching a spectrum
542 shift between 1.2 and 2 nm, followed by an additional equilibration step in analysis
543 buffer. For association measurements, all analyte samples were diluted in analysis
544 buffer at concentrations either between 3.12 and 200 nM for IgGs or between 50 and
545 3200 nM for Fab fragments. Association phases were monitored while dipping the
546 functionalized biosensors in analyte solutions for 5 min after recording a baseline for 2
547 min, and the dissociation phases monitored in analysis buffer for 10min. To assess
548 and monitor unspecific binding of analytes, measurements were performed with
549 biosensors treated with the same protocols but replacing ligand solutions with analysis
550 buffer. All measurements were performed in duplicate using sample preparations.
551 Kinetic data were processed with software provided by the manufacturer (Data
552 analysis HT v11.1). Signals from zero-concentration samples were subtracted from the
553 signals obtained for each functionalized biosensor and each analyte concentration.
554 Resulting specific kinetics signals were then fitted using a global fit method and 1:2
555 bivalent analyte model for full Abs/IgG and 1:1 Langmuir model for Fab. Reported
556 kinetics parameter values were obtained by averaging the values obtained with
557 duplicated assays and reported errors as the standard deviation.
558

559 **Crystallization of the PcrV*-Fab P3D6 complex**

560 PcrV* and P3D6 Fab were mixed in a 1:2 ratio for 1 hr at room temperature prior
561 to being subjected to size exclusion chromatography using a Superdex 200 10/300GL
562 increase column in SEC buffer (20 mM Tris pH 7.4, 150 mM NaCl, 1 mM EDTA). Peaks
563 harboring PcrV*:Fab complexes in SDS-PAGE were pooled, concentrated and used
564 for crystallization trials using the ISBG HTX crystallization platform in Grenoble. Initial
565 crystallization conditions were optimized manually (25 % PEG 1000, 1mM $ZnCl_2$, 100
566 mM sodium acetate pH 5.5), and diffracting crystals were obtained using microseeding.
567 All crystals were grown using the hanging drop vapor diffusion method at 20 °C. Single

568 crystals were mounted in cryo-loops and flash cooled in liquid nitrogen. X-ray diffraction
569 data were collected under a nitrogen stream at 100° K at the European Synchrotron
570 Facility (ESRF, Grenoble, France).

571

572 **Structure determination and refinement**

573 The best diffraction data were collected to 2.56 Å on beamline ID30A-1 (ESRF)
574 (Bowler 2015). The diffracting crystal was in space group $P2_1$ and displayed one 1:1
575 PcrV:Fab complex per asymmetric unit. Statistics on data collection and refinement
576 are summarized in supplementary table 5. X-ray diffraction images were indexed and
577 scaled with XDS (Kabsch 2010). ADXV ("Arvai, A. (2020). ADXV. A Program to Display
578 X-ray Diffraction Images. https://www.scripps.edu/tainer/arvai/adxv.html," n.d.) and
579 XDSGUI (Brehm et al., 2023) were used to perform data quality and resolution cutoff
580 check-ups (Karplus and Diederichs, 2015). The maximum possible resolution was
581 determined using the STARANISO server (Tickle, 2007). The reduced X-ray diffraction
582 data was imported into the CCP4 program suite (Agirre et al., 2023). The PcrV*-Fab
583 P3D6 structure was solved by molecular replacement using PHASER (McCoy et al.,
584 2007) and an AlphaFold2 ColabFold-generated model (Mirdita et al., 2022). The PcrV*
585 and Fab model chains were placed sequentially. The structure was completed by
586 cycles of manual model building with COOT (Emsley and Cowtan, 2004, p. 200). Water
587 molecules were added to the residual electron density map as implemented in COOT.
588 Crystallographic macromolecular refinement was performed with REFMAC
589 (Murshudov et al., 2011). Cycles of model building and refinement were performed
590 until R_{work} and R_{free} converged. The TLS definition was determined and validated using
591 the TLSMD (Painter and Merritt, 2006) and PARVATI (Zucker et al., 2010) servers.
592 The stereochemical quality of the refined models was verified with MOLPROBITY
593 (Chen et al., 2010, p. 20), PROCHECK (Laskowski et al., 1993) and PDB-REDO
594 (Joosten et al., 2014). Secondary structure assignment was performed by DSSP
595 (Kabsch and Sander, 1983) and STRIDE (Heinig and Frishman, 2004). Figures
596 displaying protein structures were generated with PYMOL (http://www.pymol.org).

597

598

ACKNOWLEDGEMENTS

This work was supported by a grant from the Agence Nationale de la Recherche (ANR-22-CE18-0009) to PP, AD and IA, as well as grant 183360 from the Région Auvergne Rhône-Alpes to PP and AD. This work used the platforms of the Grenoble Instruct-ERIC center (ISBG; UAR 3518 CNRSCEA-UGA-EMBL) within the Grenoble Partnership for Structural Biology (PSB), supported by FRISBI (ANR-10-INBS-0005-02) and GRAL, financed within the University Grenoble Alpes graduate school (Ecoles Universitaires de Recherche) CBH-EUR-GS (ANR-17-EURE-0003). The IBS acknowledges integration into the Interdisciplinary Research Institute of Grenoble (CEA).

DATA AVAILABILITY

All data generated or analyzed during this study are included in the manuscript and supporting files, with the exception of the final refined model coordinates and structure factors corresponding to the PcrV*- Fab P3D6 complex. Those were deposited in the Protein Data Bank (PDB, https://www.rcsb.org), ID code: 9FM0.

615 **REFERENCES**

616 Agirre J, Atanasova M, Bagdonas H, Ballard CB, Baslé A, Beilsten-Edmands J, Borges
617 RJ, Brown DG, Burgos-Mármol JJ, Berrisford JM, Bond PS, Caballero I, Catapano L,
618 Chojnowski G, Cook AG, Cowtan KD, Croll TI, Debreczeni JÉ, Devenish NE, Dodson
619 EJ, Drevon TR, Emsley P, Evans G, Evans PR, Fando M, Foadi J, Fuentes-Montero
620 L, Garman EF, Gerstel M, Gildea RJ, Hatti K, Hekkelman ML, Heuser P, Hoh SW,
621 Hough MA, Jenkins HT, Jiménez E, Joosten RP, Keegan RM, Keep N, Krissinel EB,
622 Kolenko P, Kovalevskiy O, Lamzin VS, Lawson DM, Lebedev AA, Leslie AGW,
623 Lohkamp B, Long F, Malý M, McCoy AJ, McNicholas SJ, Medina A, Millán C, Murray
624 JW, Murshudov GN, Nicholls RA, Noble MEM, Oeffner R, Pannu NS, Parkhurst JM,
625 Pearce N, Pereira J, Perrakis A, Powell HR, Read RJ, Rigden DJ, Rochira W, Sammito
626 M, Sánchez Rodríguez F, Sheldrick GM, Shelley KL, Simkovic F, Simpkin AJ, Skubak
627 P, Sobolev E, Steiner RA, Stevenson K, Tews I, Thomas JMH, Thorn A, Valls JT, Uski
628 V, Usón I, Vagin A, Velankar S, Vollmar M, Walden H, Waterman D, Wilson KS, Winn
629 MD, Winter G, Wojdyr M, Yamashita K. 2023. The *CCP* 4 suite: integrative software
630 for macromolecular crystallography. *Acta Crystallogr D Struct Biol* **79**:449–461.
631 doi:10.1107/S2059798323003595

632 Arvai, A. (2020). ADXV. A Program to Display X-ray Diffraction Images.
633 https://www.scripps.edu/tainer/arvai/adxv.html. n.d.

634 Berube BJ, Murphy KR, Torhan MC, Bowlin NO, Williams JD, Bowlin TL, Moir DT,
635 Hauser AR. 2017. Impact of Type III Secretion Effectors and of Phenoxyacetamide
636 Inhibitors of Type III Secretion on Abscess Formation in a Mouse Model of
637 Pseudomonas aeruginosa Infection. *Antimicrob Agents Chemother* **61**:e01202-17.
638 doi:10.1128/AAC.01202-17

639 Bowlin NO, Williams JD, Knoten CA, Torhan MC, Tashjian TF, Li B, Aiello D, Mecsas
640 J, Hauser AR, Peet NP, Bowlin TL, Moir DT. 2014. Mutations in the Pseudomonas
641 aeruginosa Needle Protein Gene *pscF* Confer Resistance to Phenoxyacetamide
642 Inhibitors of the Type III Secretion System. *Antimicrob Agents Chemother* **58**:2211–
643 2220. doi:10.1128/AAC.02795-13

644 Brehm W, Triviño J, Krahn JM, Usón I, Diederichs K. 2023. *XDSGUI* : a graphical user
645 interface for *XDS* , *SHELX* and *ARCIMBOLDO*. *J Appl Crystallogr* **56**:1585–1594.
646 doi:10.1107/S1600576723007057

647 Charpentier X, Oswald E. 2004. Identification of the Secretion and Translocation
648 Domain of the Enteropathogenic and Enterohemorrhagic *Escherichia coli* Effector Cif,
649 Using TEM-1 β-Lactamase as a New Fluorescence-Based Reporter. *J Bacteriol*
650 **186**:5486–5495. doi:10.1128/JB.186.16.5486-5495.2004

651 Chastre J, François B, Bourgeois M, Komnos A, Ferrer R, Rahav G, De Schryver N,
652 Lepape A, Koksal I, Luyt C-E, Sánchez-García M, Torres A, Eggimann P, Koulenti D,

Holland TL, Ali O, Shoemaker K, Ren P, Sauser J, Ruzin A, Tabor DE, Akhgar A, Wu Y, Jiang Y, DiGiandomenico A, Colbert S, Vandamme D, Coenjaerts F, Malhotra-Kumar S, Timbermont L, Oliver A, Barraud O, Bellamy T, Bonten M, Goossens H, Reisner C, Esser MT, Jafri HS, The COMBACTE-MAGNET EVADE Study Group, Joannidis M, Klimscha W, De Waele E, Devriendt J, Huberlant V, Depuydt P, Van Boxstael S, Peric M, Kopic J, Hanauer M, Hruby T, Sramek V, Svoboda P, Vymazal T, Novacek M, Annane D, Mira J-P, Souweine B, Dequin P-F, Meziani F, Stephan F, Nseir S, Gibot S, Schwebel C, Plantefeve G, Diehl J-L, Richard C, Lamer C, Klouche K, Jaber S, Zakynthinos E, Filntisis G, Zakynthinos S, Koutsoukou A, Saroglou G, Nikolaou C, Vlachogianni G, Pnevmatikos I, Mandragos K, Kremer I, Rozgonyi ZD, Marjanek Z, Martin-Loeches I, Singer P, Van Heerden V, Carmeli Y, Povoa P, Seoane AA, Moura P, Gonzalez F, Ramirez P, Marti AT, Roca RF, Oteiza L, Escudero D, Piacentini E, Vera P, Tamayo L, Gallego MAG, Canas BS, Figueira I, Leon R, Korten V, Akova M, Wyncoll D, Whitehouse T, Hopkins P, Sim M, Golan Y, Zervos M, Vazquez J, Cherabuddi K, Smulian G, Rouphael N, Welker J, Sims M, Van Duin D, McCarthy T, Polk C. 2022. Safety, efficacy, and pharmacokinetics of gremubamab (MEDI3902), an anti-Pseudomonas aeruginosa bispecific human monoclonal antibody, in P. aeruginosa-colonised, mechanically ventilated intensive care unit patients: a randomised controlled trial. *Crit Care* **26**:355. doi:10.1186/s13054-022-04204-9

Chen VB, Arendall WB, Headd JJ, Keedy DA, Immormino RM, Kapral GJ, Murray LW, Richardson JS, Richardson DC. 2010. *MolProbity*: all-atom structure validation for macromolecular crystallography. *Acta Crystallogr D Biol Crystallogr* **66**:12–21. doi:10.1107/S0907444909042073

Cisz M, Lee P-C, Rietsch A. 2008. ExoS Controls the Cell Contact-Mediated Switch to Effector Secretion in *Pseudomonas aeruginosa*. *J Bacteriol* **190**:2726–2738. doi:10.1128/JB.01553-07

Coburn B, Sekirov I, Finlay BB. 2007. Type III Secretion Systems and Disease. *Clin Microbiol Rev* **20**:535–549. doi:10.1128/CMR.00013-07

Crowe JE. 2022. Human Antibodies for Viral Infections. *Annu Rev Immunol* **40**:349–386. doi:10.1146/annurev-immunol-042718-041309

Dacheux D, Goure J, Chabert J, Usson Y, Attree I. 2001. Pore-forming activity of type III system-secreted proteins leads to oncosis of *Pseudomonas aeruginosa* -infected macrophages. *Molecular Microbiology* **40**:76–85. doi:10.1046/j.1365-2958.2001.02368.x

De Melo AG, Morency C, Moineau S. 2024. Virulence-associated factors as targets for phage infection. *Current Opinion in Microbiology* **79**:102471. doi:10.1016/j.mib.2024.102471

690 Derewenda ZS. 2011. It's all in the crystals…. *Acta Crystallogr D Biol Crystallogr*
691 **67**:243–248. doi:10.1107/S0907444911007797

692 Diepold A, Wagner S. 2014. Assembly of the bacterial type III secretion machinery.
693 *FEMS Microbiol Rev* **38**:802–822. doi:10.1111/1574-6976.12061

694 DiGiandomenico A, Keller AE, Gao Cuihua, Rainey GJ, Warrener P, Camara MM,
695 Bonnell J, Fleming R, Bezabeh B, Dimasi N, Sellman BR, Hilliard J, Guenther CM,
696 Datta V, Zhao W, Gao Changshou, Yu X-Q, Suzich JA, Stover CK. 2014. A
697 multifunctional bispecific antibody protects against *Pseudomonas aeruginosa*. *Sci*
698 *Transl Med* **6**. doi:10.1126/scitranslmed.3009655

699 Dortet L, Lombardi C, Cretin F, Dessen A, Filloux A. 2018. Pore-forming activity of the
700 Pseudomonas aeruginosa type III secretion system translocon alters the host
701 epigenome. *Nat Microbiol* **3**:378–386. doi:10.1038/s41564-018-0109-7

702 Duan L, Zhang J, Chen Z, Gou Q, Xiong Q, Yuan Y, Jing H, Zhu J, Ni L, Zheng Y, Liu
703 Z, Zhang X, Zeng H, Zou Q, Zhao Z. 2021. Antibiotic Combined with Epitope-Specific
704 Monoclonal Antibody Cocktail Protects Mice Against Bacteremia and Acute
705 Pneumonia from Methicillin-Resistant Staphylococcus aureus Infection. *JIR* **Volume**
706 **14**:4267–4282. doi:10.2147/JIR.S325286

707 Emsley P, Cowtan K. 2004. *Coot* : model-building tools for molecular graphics. *Acta*
708 *Crystallogr D Biol Crystallogr* **60**:2126–2132. doi:10.1107/S0907444904019158

709 Erskine PT, Knight MJ, Ruaux A, Mikolajek H, Sang NWF, Withers J, Gill R, Wood SP,
710 Wood M, Fox GC, Cooper JB. 2006. High Resolution Structure of BipD: An Invasion
711 Protein Associated with the Type III Secretion System of Burkholderia Pseudomallei.
712 *Journal of Molecular Biology* **363**:125–136. doi:10.1016/j.jmb.2006.07.069

713 Faudry E, Vernier G, Neumann E, Forge V, Attree I. 2006. Synergistic Pore Formation
714 by Type III Toxin Translocators of *Pseudomonas aeruginosa*. *Biochemistry* **45**:8117–
715 8123. doi:10.1021/bi060452+

716 François B, Luyt C-E, Dugard A, Wolff M, Diehl J-L, Jaber S, Forel J-M, Garot D, Kipnis
717 E, Mebazaa A, Misset B, Andremont A, Ploy M-C, Jacobs A, Yarranton G, Pearce T,
718 Fagon J-Y, Chastre J. 2012. Safety and pharmacokinetics of an anti-PcrV PEGylated
719 monoclonal antibody fragment in mechanically ventilated patients colonized with
720 Pseudomonas aeruginosa: A randomized,double-blind, placebo-controlled trial*.
721 *Critical Care Medicine* **40**:2320–2326. doi:10.1097/CCM.0b013e31825334f6

722 Frank DW, Vallis A, Wiener-Kronish JP, Roy-Burman A, Spack EG, Mullaney BP,
723 Megdoud M, Marks JD, Fritz R, Sawa T. 2002. Generation and Characterization of a
724 Protective Monoclonal Antibody to *Pseudomonas aeruginosa* PcrV. *J INFECT DIS*
725 **186**:64–73. doi:10.1086/341069

726 Gébus C, Faudry E, Bohn Y-ST, Elsen S, Attree I. 2009. Oligomerization of PcrV and
727 LcrV, protective antigens of Pseudomonas aeruginosa and Yersinia pestis. *Journal of*
728 *Biological Chemistry* **284**:21776. doi:10.1074/jbc.A803146200

729 Goure J, Broz P, Attree O, Cornelis GR, Attree I. 2005. Protective Anti-V Antibodies
730 Inhibit *Pseudomonas* and *Yersinia* Translocon Assembly within Host Membranes. *J*
731 *INFECT DIS* **192**:218–225. doi:10.1086/430932

732 Goure J, Pastor A, Faudry E, Chabert J, Dessen A, Attree I. 2004. The V Antigen of
733 *Pseudomonas aeruginosa* Is Required for Assembly of the Functional PopB/PopD
734 Translocation Pore in Host Cell Membranes. *Infect Immun* **72**:4741–4750.
735 doi:10.1128/IAI.72.8.4741-4750.2004

736 Guo EZ, Galán JE. 2021. Cryo-EM structure of the needle filament tip complex of the
737 *Salmonella* type III secretion injectisome. *Proc Natl Acad Sci USA* **118**:e2114552118.
738 doi:10.1073/pnas.2114552118

739 Habenstein B, El Mammeri N, Tolchard J, Lamon G, Tawani A, Berbon M, Loquet A.
740 2019. Structures of Type III Secretion System Needle Filaments In: Wagner S, Galan
741 JE, editors. Bacterial Type III Protein Secretion Systems, Current Topics in
742 Microbiology and Immunology. Cham: Springer International Publishing. pp. 109–131.
743 doi:10.1007/82_2019_192

744 Hauser AR. 2009. The type III secretion system of Pseudomonas aeruginosa: infection
745 by injection. *Nat Rev Microbiol* **7**:654–665. doi:10.1038/nrmicro2199

746 Heinig M, Frishman D. 2004. STRIDE: a web server for secondary structure
747 assignment from known atomic coordinates of proteins. *Nucleic Acids Research*
748 **32**:W500–W502. doi:10.1093/nar/gkh429

749 Horcajada JP, Montero M, Oliver A, Sorlí L, Luque S, Gómez-Zorrilla S, Benito N, Grau
750 S. 2019. Epidemiology and Treatment of Multidrug-Resistant and Extensively Drug-
751 Resistant Pseudomonas aeruginosa Infections. *Clin Microbiol Rev* **32**:e00031-19.
752 doi:10.1128/CMR.00031-19

753 Hu Y, Huang H, Cheng X, Shu X, White AP, Stavrinides J, Köster W, Zhu G, Zhao Z,
754 Wang Y. 2017. A global survey of bacterial type III secretion systems and their
755 effectors. *Environmental Microbiology* **19**:3879–3895. doi:10.1111/1462-2920.13755

756 Imamura Y, Yanagihara K, Fukuda Y, Kaneko Y, Seki M, Izumikawa K, Miyazaki Y,
757 Hirakata Y, Sawa T, Wiener-Kronish JP, Kohno S. 2007. Effect of anti-PcrV antibody
758 in a murine chronic airway Pseudomonas aeruginosa infection model. *European*
759 *Respiratory Journal* **29**:965–968. doi:10.1183/09031936.00147406

760 Jain R, Beckett VV, Konstan MW, Accurso FJ, Burns JL, Mayer-Hamblett N, Milla C,
761 VanDevanter DR, Chmiel JF. 2018. KB001-A, a novel anti-inflammatory, found to be

safe and well-tolerated in cystic fibrosis patients infected with Pseudomonas aeruginosa. *Journal of Cystic Fibrosis* **17**:484–491. doi:10.1016/j.jcf.2017.12.006

Joosten RP, Long F, Murshudov GN, Perrakis A. 2014. The *PDB_REDO* server for macromolecular structure model optimization. *IUCrJ* **1**:213–220. doi:10.1107/S2052252514009324

Kabsch W, Sander C. 1983. Dictionary of protein secondary structure: Pattern recognition of hydrogen-bonded and geometrical features. *Biopolymers* **22**:2577–2637. doi:10.1002/bip.360221211

Karplus PA, Diederichs K. 2015. Assessing and maximizing data quality in macromolecular crystallography. *Current Opinion in Structural Biology* **34**:60–68. doi:10.1016/j.sbi.2015.07.003

Kaufmann SHE, Dorhoi A, Hotchkiss RS, Bartenschlager R. 2018. Host-directed therapies for bacterial and viral infections. *Nat Rev Drug Discov* **17**:35–56. doi:10.1038/nrd.2017.162

Kundracik E, Trichka J, Díaz Aponte J, Roistacher A, Rietsch A. 2022. PopB-PcrV Interactions Are Essential for Pore Formation in the Pseudomonas aeruginosa Type III Secretion System Translocon. *mBio* **13**:e02381-22. doi:10.1128/mbio.02381-22

La Guidara C, Adamo R, Sala C, Micoli F. 2024. Vaccines and Monoclonal Antibodies as Alternative Strategies to Antibiotics to Fight Antimicrobial Resistance. *IJMS* **25**:5487. doi:10.3390/ijms25105487

Laskowski RA, MacArthur MW, Moss DS, Thornton JM. 1993. PROCHECK: a program to check the stereochemical quality of protein structures. *J Appl Crystallogr* **26**:283–291. doi:10.1107/S0021889892009944

Lee P, Stopford CM, Svenson AG, Rietsch A. 2010. Control of effector export by the *Pseudomonas aeruginosa* type III secretion proteins PcrG and PcrV. *Molecular Microbiology* **75**:924–941. doi:10.1111/j.1365-2958.2009.07027.x

Levin MJ, Ustianowski A, De Wit S, Launay O, Avila M, Templeton A, Yuan Y, Seegobin S, Ellery A, Levinson DJ, Ambery P, Arends RH, Beavon R, Dey K, Garbes P, Kelly EJ, Koh GCKW, Near KA, Padilla KW, Psachoulia K, Sharbaugh A, Streicher K, Pangalos MN, Esser MT. 2022. Intramuscular AZD7442 (Tixagevimab–Cilgavimab) for Prevention of Covid-19. *N Engl J Med* **386**:2188–2200. doi:10.1056/NEJMoa2116620

Lunelli M, Hurwitz R, Lambers J, Kolbe M. 2011. Crystal Structure of PrgI-SipD: Insight into a Secretion Competent State of the Type Three Secretion System Needle Tip and its Interaction with Host Ligands. *PLoS Pathog* **7**:e1002163. doi:10.1371/journal.ppat.1002163

Matteï P, Faudry E, Job V, Izoré T, Attree I, Dessen A. 2011. Membrane targeting and pore formation by the type III secretion system translocon. *The FEBS Journal* **278**:414–426. doi:10.1111/j.1742-4658.2010.07974.x

McCoy AJ, Grosse-Kunstleve RW, Adams PD, Winn MD, Storoni LC, Read RJ. 2007. *Phaser* crystallographic software. *J Appl Crystallogr* **40**:658–674. doi:10.1107/S0021889807021206

Mirdita M, Schütze K, Moriwaki Y, Heo L, Ovchinnikov S, Steinegger M. 2022. ColabFold: making protein folding accessible to all. *Nat Methods* **19**:679–682. doi:10.1038/s41592-022-01488-1

Montagner C, Arquint C, Cornelis GR. 2011. Translocators YopB and YopD from Yersinia enterocolitica Form a Multimeric Integral Membrane Complex in Eukaryotic Cell Membranes. *J Bacteriol* **193**:6923–6928. doi:10.1128/JB.05555-11

Morrison C. 2015. Antibacterial antibodies gain traction. *Nat Rev Drug Discov* **14**:737–738. doi:10.1038/nrd4770

Mueller CA, Broz P, Cornelis GR. 2008. The type III secretion system tip complex and translocon. *Molecular Microbiology* **68**:1085–1095. doi:10.1111/j.1365-2958.2008.06237.x

Mulangu S, Dodd LE, Davey RT, Tshiani Mbaya O, Proschan M, Mukadi D, Lusakibanza Manzo M, Nzolo D, Tshomba Oloma A, Ibanda A, Ali R, Coulibaly S, Levine AC, Grais R, Diaz J, Lane HC, Muyembe-Tamfum J-J. 2019. A Randomized, Controlled Trial of Ebola Virus Disease Therapeutics. *N Engl J Med* **381**:2293–2303. doi:10.1056/NEJMoa1910993

Murray CJL, Ikuta KS, Sharara F, Swetschinski L, Robles Aguilar G, Gray A, Han C, Bisignano C, Rao P, Wool E, Johnson SC, Browne AJ, Chipeta MG, Fell F, Hackett S, Haines-Woodhouse G, Kashef Hamadani BH, Kumaran EAP, McManigal B, Achalapong S, Agarwal R, Akech S, Albertson S, Amuasi J, Andrews J, Aravkin A, Ashley E, Babin F-X, Bailey F, Baker S, Basnyat B, Bekker A, Bender R, Berkley JA, Bethou A, Bielicki J, Boonkasidecha S, Bukosia J, Carvalheiro C, Castañeda-Orjuela C, Chansamouth V, Chaurasia S, Chiurchiù S, Chowdhury F, Clotaire Donatien R, Cook AJ, Cooper B, Cressey TR, Criollo-Mora E, Cunningham M, Darboe S, Day NPJ, De Luca M, Dokova K, Dramowski A, Dunachie SJ, Duong Bich T, Eckmanns T, Eibach D, Emami A, Feasey N, Fisher-Pearson N, Forrest K, Garcia C, Garrett D, Gastmeier P, Giref AZ, Greer RC, Gupta V, Haller S, Haselbeck A, Hay SI, Holm M, Hopkins S, Hsia Y, Iregbu KC, Jacobs J, Jarovsky D, Javanmardi F, Jenney AWJ, Khorana M, Khusuwan S, Kissoon N, Kobeissi E, Kostyanev T, Krapp F, Krumkamp R, Kumar A, Kyu HH, Lim C, Lim K, Limmathurotsakul D, Loftus MJ, Lunn M, Ma J, Manoharan A, Marks F, May J, Mayxay M, Mturi N, Munera-Huertas T, Musicha P, Musila LA, Mussi-Pinhata MM, Naidu RN, Nakamura T, Nanavati R, Nangia S, Newton P, Ngoun C,

Novotney A, Nwakanma D, Obiero CW, Ochoa TJ, Olivas-Martinez A, Olliaro P, Ooko E, Ortiz-Brizuela E, Ounchanum P, Pak GD, Paredes JL, Peleg AY, Perrone C, Phe T, Phommasone K, Plakkal N, Ponce-de-Leon A, Raad M, Ramdin T, Rattanavong S, Riddell A, Roberts T, Robotham JV, Roca A, Rosenthal VD, Rudd KE, Russell N, Sader HS, Saengchan W, Schnall J, Scott JAG, Seekaew S, Sharland M, Shivamallappa M, Sifuentes-Osornio J, Simpson AJ, Steenkeste N, Stewardson AJ, Stoeva T, Tasak N, Thaiprakong A, Thwaites G, Tigoi C, Turner C, Turner P, Van Doorn HR, Velaphi S, Vongpradith A, Vongsouvath M, Vu H, Walsh T, Walson JL, Waner S, Wangrangsimakul T, Wannapinij P, Wozniak T, Young Sharma TEMW, Yu KC, Zheng P, Sartorius B, Lopez AD, Stergachis A, Moore C, Dolecek C, Naghavi M. 2022. Global burden of bacterial antimicrobial resistance in 2019: a systematic analysis. *The Lancet* **399**:629–655. doi:10.1016/S0140-6736(21)02724-0

Murshudov GN, Skubák P, Lebedev AA, Pannu NS, Steiner RA, Nicholls RA, Winn MD, Long F, Vagin AA. 2011. *REFMAC* 5 for the refinement of macromolecular crystal structures. *Acta Crystallogr D Biol Crystallogr* **67**:355–367. doi:10.1107/S0907444911001314

Nanao M, Ricard-Blum S, Di Guilmi A, Lemaire D, Lascoux D, Chabert J, Attree I, Dessen A. 2003. [No title found]. *BMC Microbiol* **3**:21. doi:10.1186/1471-2180-3-21

Ngo T-D, Plé S, Thomas A, Barette C, Fortuné A, Bouzidi Y, Fauvarque M-O, Pereira De Freitas R, Francisco Hilário F, Attrée I, Wong Y-S, Faudry E. 2019. Chimeric Protein–Protein Interface Inhibitors Allow Efficient Inhibition of Type III Secretion Machinery and *Pseudomonas aeruginosa* Virulence. *ACS Infect Dis* **5**:1843–1854. doi:10.1021/acsinfecdis.9b00154

Painter J, Merritt EA. 2006. *TLSMD* web server for the generation of multi-group TLS models. *J Appl Crystallogr* **39**:109–111. doi:10.1107/S0021889805038987

Pennini ME, De Marco A, Pelletier M, Bonnell J, Cvitkovic R, Beltramello M, Cameroni E, Bianchi S, Zatta F, Zhao W, Xiao X, Camara MM, DiGiandomenico A, Semenova E, Lanzavecchia A, Warrener P, Suzich J, Wang Q, Corti D, Stover CK. 2017. Immune stealth-driven O2 serotype prevalence and potential for therapeutic antibodies against multidrug resistant Klebsiella pneumoniae. *Nat Commun* **8**:1991. doi:10.1038/s41467-017-02223-7

Quinaud M, Chabert J, Faudry E, Neumann E, Lemaire D, Pastor A, Elsen S, Dessen A, Attree I. 2005. The PscE-PscF-PscG Complex Controls Type III Secretion Needle Biogenesis in Pseudomonas aeruginosa. *Journal of Biological Chemistry* **280**:36293–36300. doi:10.1074/jbc.M508089200

Quinaud M, Plé S, Job V, Contreras-Martel C, Simorre J-P, Attree I, Dessen A. 2007. Structure of the heterotrimeric complex that regulates type III secretion needle formation. *Proc Natl Acad Sci USA* **104**:7803–7808. doi:10.1073/pnas.0610098104

874 Rollenske T, Szijarto V, Lukasiewicz J, Guachalla LM, Stojkovic K, Hartl K, Stulik L,
875 Kocher S, Lasitschka F, Al-Saeedi M, Schröder-Braunstein J, Von Frankenberg M,
876 Gaebelein G, Hoffmann P, Klein S, Heeg K, Nagy E, Nagy G, Wardemann H. 2018.
877 Cross-specificity of protective human antibodies against Klebsiella pneumoniae LPS
878 O-antigen. *Nat Immunol* **19**:617–624. doi:10.1038/s41590-018-0106-2

879 Roy-Burman A, Savel RH, Racine S, Swanson BL, Revadigar NS, Fujimoto J, Sawa
880 T, Frank DW, Wiener-Kronish JP. 2001. Type III Protein Secretion Is Associated with
881 Death in Lower Respiratory and Systemic *Pseudomonas aeruginosa* Infections. *J*
882 *INFECT DIS* **183**:1767–1774. doi:10.1086/320737

883 Sawa, Kinoshita, Inoue, Ohara, Moriyama. 2019. Immunoglobulin for Treating
884 Bacterial Infections: One More Mechanism of Action. *Antibodies* **8**:52.
885 doi:10.3390/antib8040052
886

887 Schoehn G, Di Guilmi AM, Lemaire D, Attree I, Weissenhorn W, Dessen A. 2003.
888 Oligomerization of type III secretion proteins PopB and PopD precedes pore formation
889 in Pseudomonas. *EMBO J*. **22**(19):4957-67. doi:10.1093/emboj/cdg499.

890 Serapio-Palacios A, Finlay BB. 2020. Dynamics of expression, secretion and
891 translocation of type III effectors during enteropathogenic Escherichia coli infection.
892 *Current Opinion in Microbiology* **54**:67–76. doi:10.1016/j.mib.2019.12.001

893 Simonis A, Kreer C, Albus A, Rox K, Yuan B, Holzmann D, Wilms JA, Zuber S, Kottege
894 L, Winter S, Meyer M, Schmitt K, Gruell H, Theobald SJ, Hellmann A-M, Meyer C,
895 Ercanoglu MS, Cramer N, Munder A, Hallek M, Fätkenheuer G, Koch M, Seifert H,
896 Rietschel E, Marlovits TC, Van Koningsbruggen-Rietschel S, Klein F, Rybniker J. 2023.
897 Discovery of highly neutralizing human antibodies targeting Pseudomonas aeruginosa.
898 *Cell* **186**:5098-5113.e19. doi:10.1016/j.cell.2023.10.002

899 Tabor DE, Oganesyan V, Keller AE, Yu L, McLaughlin RE, Song E, Warrener P,
900 Rosenthal K, Esser M, Qi Y, Ruzin A, Stover CK, DiGiandomenico A. 2018.
901 Pseudomonas aeruginosa PcrV and Psl, the Molecular Targets of Bispecific Antibody
902 MEDI3902, Are Conserved Among Diverse Global Clinical Isolates. *The Journal of*
903 *Infectious Diseases*. doi:10.1093/infdis/jiy438

904 Tickle IJ. 2007. Experimental determination of optimal root-mean-square deviations of
905 macromolecular bond lengths and angles from their restrained ideal values. *Acta*
906 *Crystallogr D Biol Crystallogr* **63**:1274–1281. doi:10.1107/S0907444907050196

907 Vacca F, Sala C, Rappuoli R. 2022. Monoclonal Antibodies for Bacterial Pathogens:
908 Mechanisms of Action and Engineering Approaches for Enhanced Effector Functions.
909 *Biomedicines* **10**:2126. doi:10.3390/biomedicines10092126

910 Verove J, Bernarde C, Bohn Y-ST, Boulay F, Rabiet M-J, Attree I, Cretin F. 2012.
911 Injection of Pseudomonas aeruginosa Exo Toxins into Host Cells Can Be Modulated
912 by Host Factors at the Level of Translocon Assembly and/or Activity. *PLoS ONE*
913 **7**:e30488. doi:10.1371/journal.pone.0030488

914 Watson A, Li H, Ma B, Weiss R, Bendayan D, Abramovitz L, Ben-Shalom N, Mor M,
915 Pinko E, Bar Oz M, Wang Z, Du F, Lu Y, Rybniker J, Dahan R, Huang H, Barkan D,
916 Xiang Y, Javid B, Freund NT. 2021. Human antibodies targeting a Mycobacterium
917 transporter protein mediate protection against tuberculosis. *Nat Commun* **12**:602.
918 doi:10.1038/s41467-021-20930-0

919 West SEH, Schweizer HP, Dall C, Sample AK, Runyen-Janecky LJ. 1994.
920 Construction of improved Escherichia-Pseudomonas shuttle vectors derived from
921 pUC18/19 and sequence of the region required for their replication in Pseudomonas
922 aeruginosa. *Gene* **148**:81–86. doi:10.1016/0378-1119(94)90237-2

923 Yaeger LN, Coles VE, Chan DCK, Burrows LL. 2021. How to kill *Pseudomonas* —
924 emerging therapies for a challenging pathogen. *Annals of the New York Academy of*
925 *Sciences* **1496**:59–81. doi:10.1111/nyas.14596

926 Zucker F, Champ PC, Merritt EA. 2010. Validation of crystallographic models
927 containing TLS or other descriptions of anisotropy. *Acta Crystallogr D Biol Crystallogr*
928 **66**:889–900. doi:10.1107/S0907444910020421

929
930

931 **FIGURES**

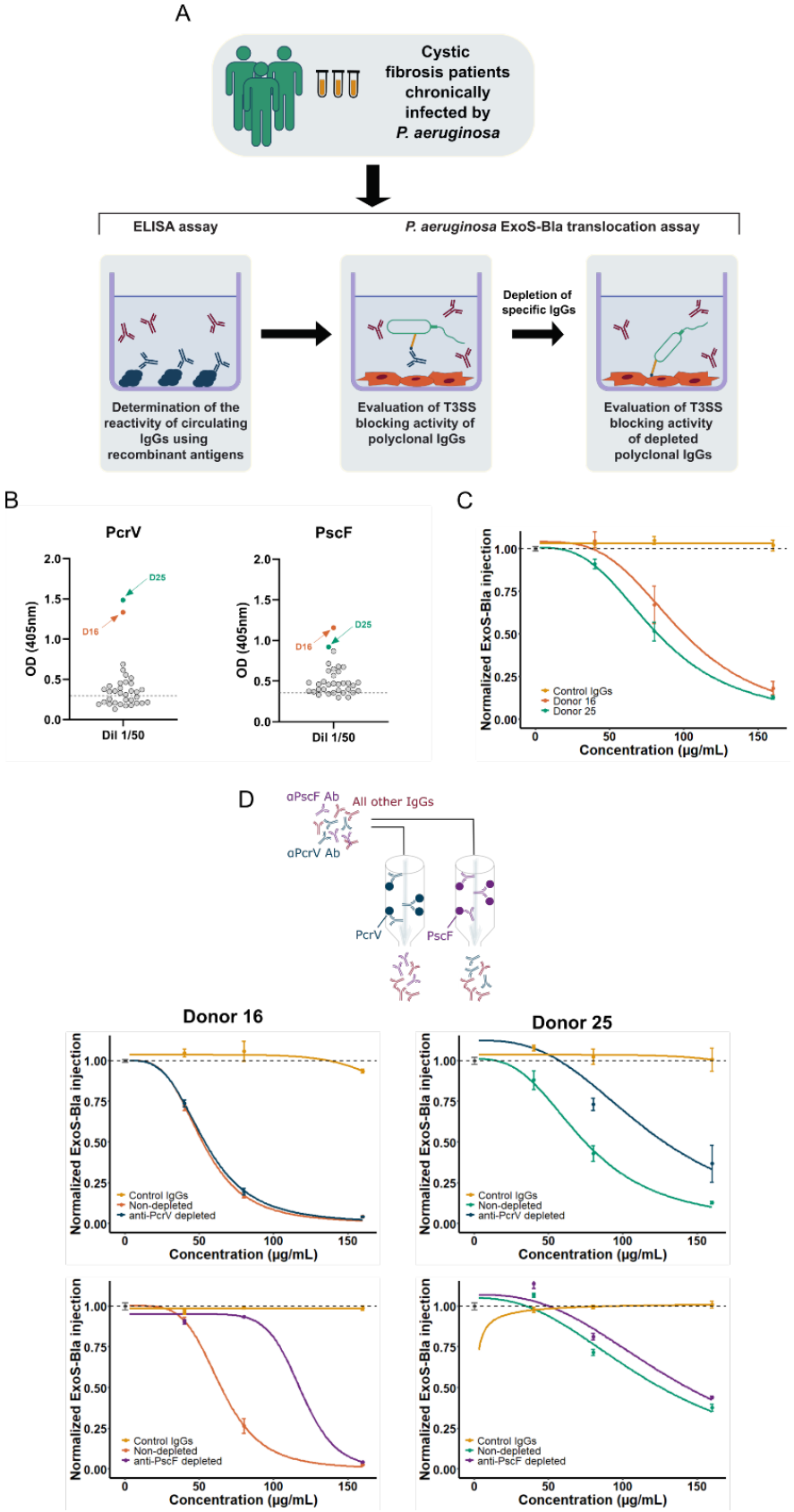

932

933 **Figure 1. Screening workflow and donor selection**

934 (A) Schematic representation of the workflow from patient selection to evaluation of
935 T3SS-blocking activity. (B) ELISA results indicating that sera of donors 16 and 25

936 possess the highest Ab titers against recombinant PcrV and PscF. (C) ExoS-Bla
937 translocation blocking activity of serum from donors 16 and 25. (D) (top) scheme of
938 depletion experiment of specific Abs on either PscF- or PcrV–loaded columns. (bottom)
939 blocking activity of depleted sera for both donors.

A

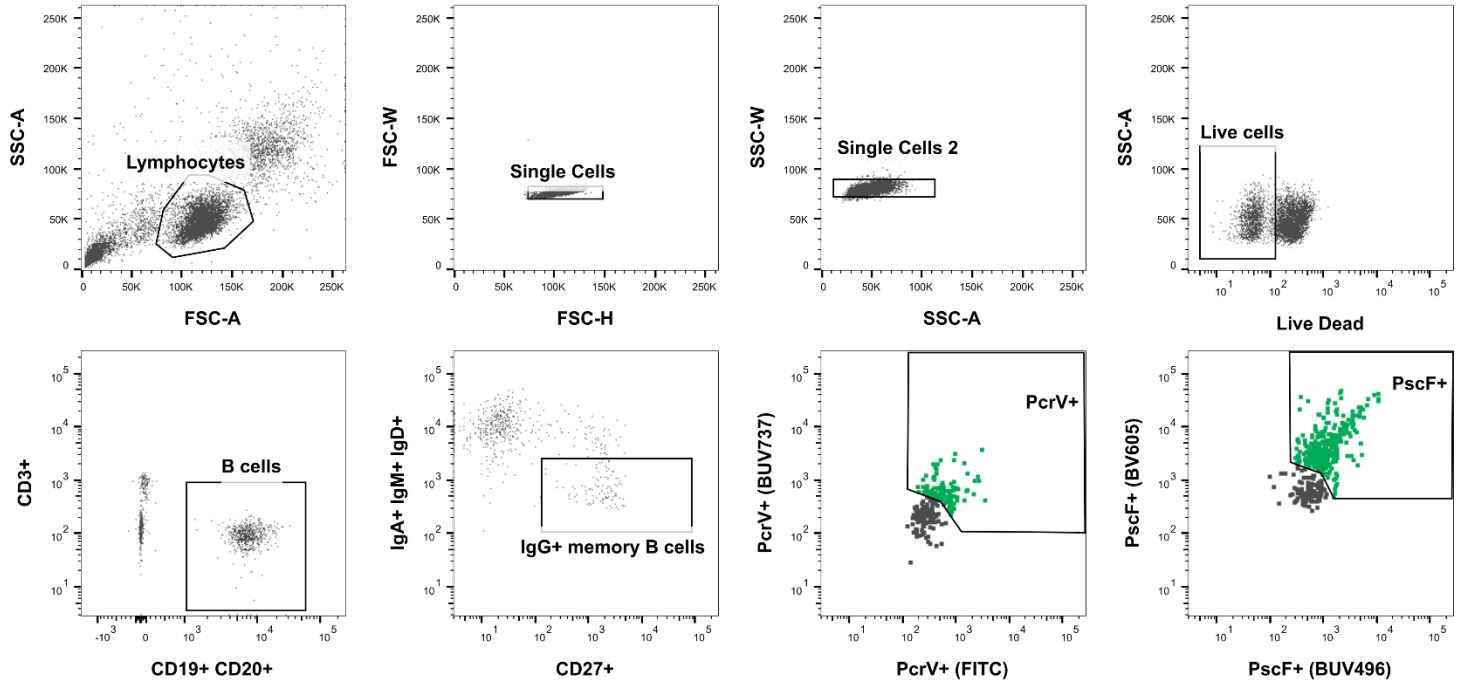

B

Anti-PcrV mAbs	EC_{50} (µg/mL)	ExoS-Bla inhibition
P3D6	0.03	24 %
P5B3	0.04	94 %
P3G9	0.08	No inhibition
P5E10	0.17	No inhibition
Anti-PscF mAbs	EC_{50} (µg/mL)	ExoS-Bla inhibition
P5G10	0.01	No inhibition
P1B7	0.07	No inhibition
P5D5	0.07	No inhibition
P1D5	0.18	No inhibition
P1B4	0.24	No inhibition
P3G6	1.28	No inhibition
P3G2	2.08	No inhibition
P1F5	4.65	No inhibition
P3G7	10.61	No inhibition
P1D7	>30	No inhibition

Figure 2. Selection of B cells from donors 16 and 25. (A) B cells sorting and isolation using PscF and PcrV baits. (B) Table summarizing the EC_{50} values of selected Abs obtained by ELISA and the percentage of inhibition of ExoS-Bla injection into epithelial cells at 100 µg/mL.

A

Variant	Amino acid positions			
	6	9	21	225
V1 (PAO1-like)	Leu	Ala	Ser	Ser
V2 (CHA-like)	Leu	Ala	Ser	Arg
V3 (PA14-like)	Phe	Ala	Pro	Lys
V4 (PA103-like)	Phe	Gly	Pro	Arg
V5	Phe	Gly	Pro	Lys

B

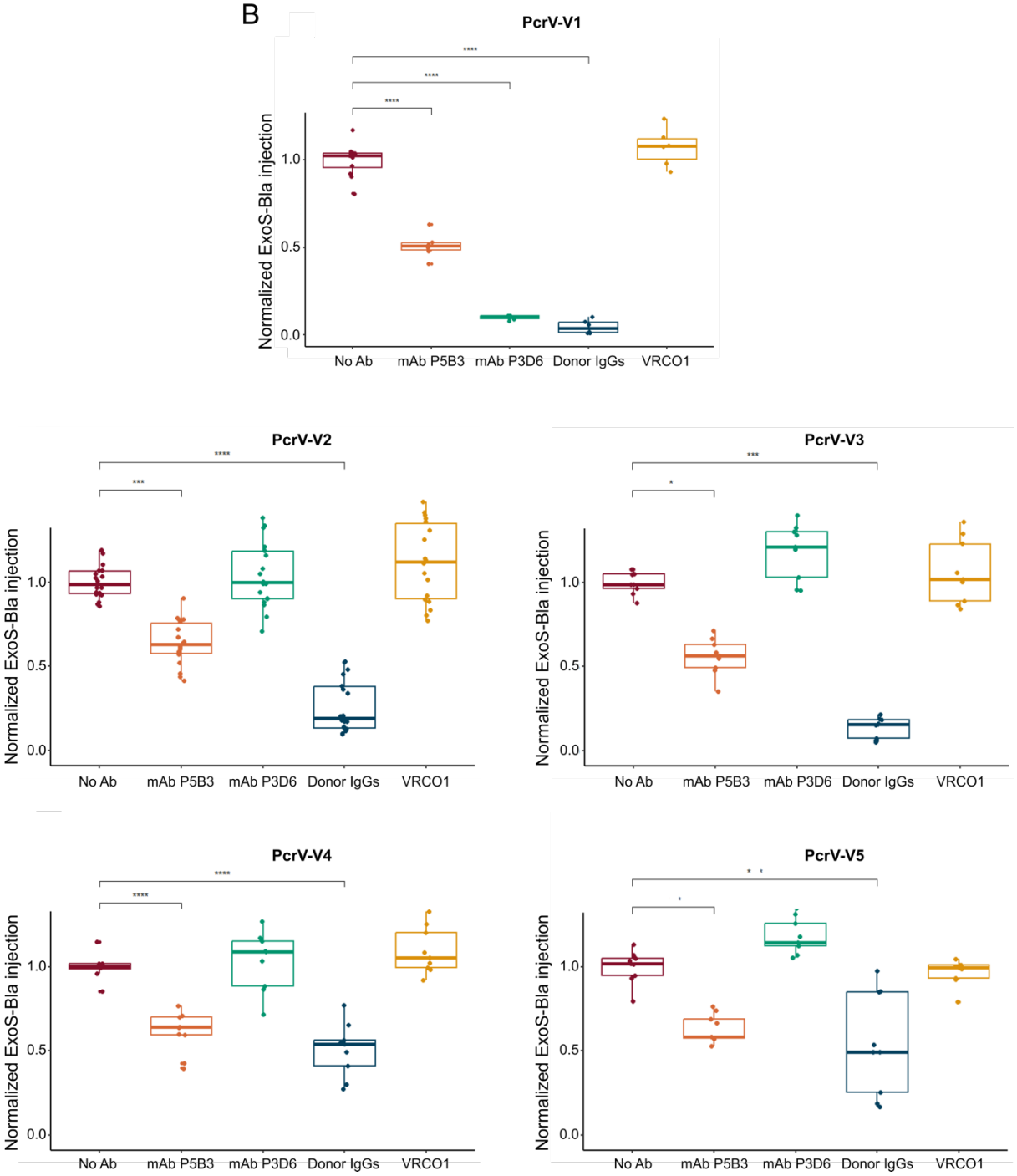

Figure 3. **mAbs P5B3 and P3D6 activity on PcrV variants**. (A) PcrV variability in clinical strains. The most variable position (225) can either be Ser, Arg or Lys. Representative strains are indicated when available (PAO1 for V1, CHA for V2, PA14

951 for V3 and PA103 for V4). (B) Inhibition of ExoS-Bla activity following infection of A549
952 epithelial cells with *P. aeruginosa* expressing the V1 variant. IgGs from donor 25, as
953 well as mAbs P5B3 and P3D6 block ExoS-Bla injection, while the control mAb VRCO1
954 is inefficient. While P3D6 displays significant inhibition only towards V1, P5B3 displays
955 dose-dependent inhibition on all five variants (see also Supplementary Figure 1).

956

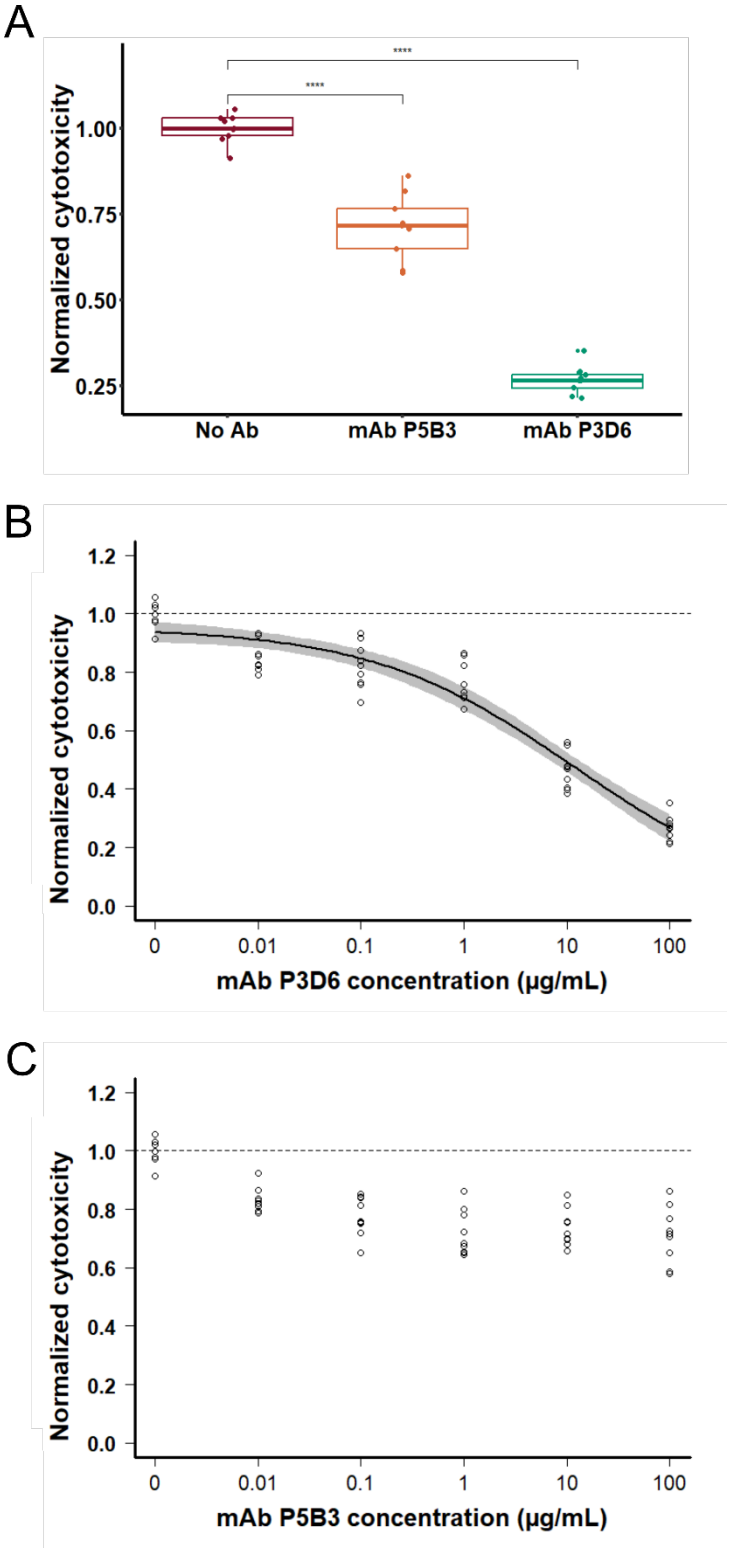

Figure 4. mAb P3D6 efficiently inhibits the PopB/PopD translocation pore. J774 macrophages were infected with *P. aeruginosa* strain (PAO1, V1) deprived of all three T3SS toxins. The cell death (cytotoxicity) resulting from insertion of the translocon pore was measured by propidium iodide incorporation and normalized to the wild-type strain without addition of mAbs. (A) Both P3D6 and P5B3 mAbs significantly reduce pore formation at 100 µg/mL. (B, C) Only P3D6 exhibits a significant dose-response inhibitory effect on cytotoxicity towards J774 cells with an IC_{50} of 11.8 µg/mL.

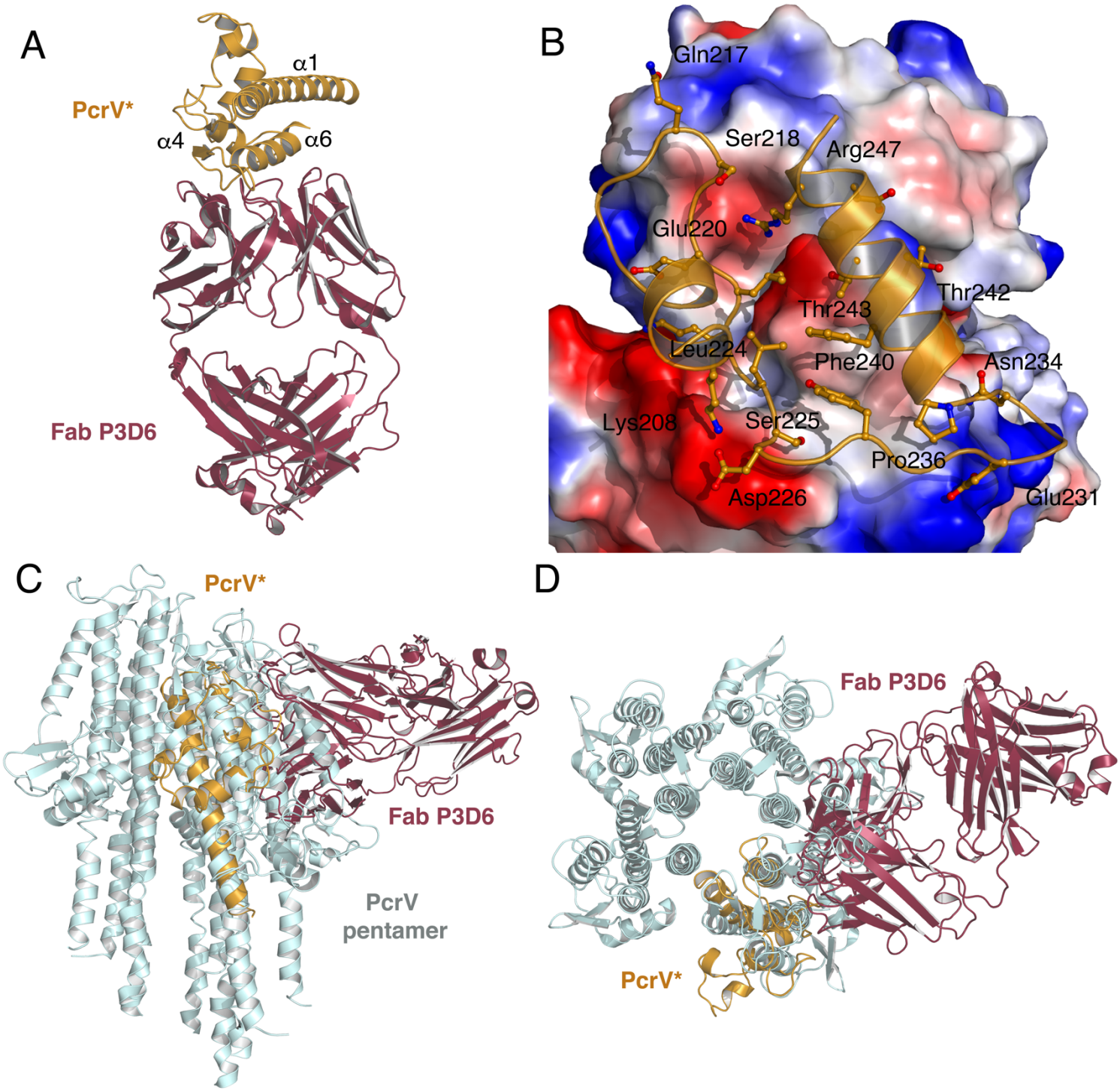

Figure 5. Structure of Fab P3D6 in complex with PcrV*. (A) Crystal structure of Fab P3D6 in complex with PcrV*. Fab P3D6 is shown in brown, while PcrV* is in orange. Contacts are made between PcrV* and an interaction platform formed by both HC and LC of P3D6. (B) Closeup of the interaction between PcrV* and P3D6, with the latter being shown as an electrostatic surface where acidic regions are shown in red, and basic in blue. Side (C) and top (D) views of the modeled PcrV pentamer, in light blue) onto which the structure shown in (A) was overlaid. Note that the bound Fab clashes with a neighboring PcrV protomer, precluding the formation of the pentamer.

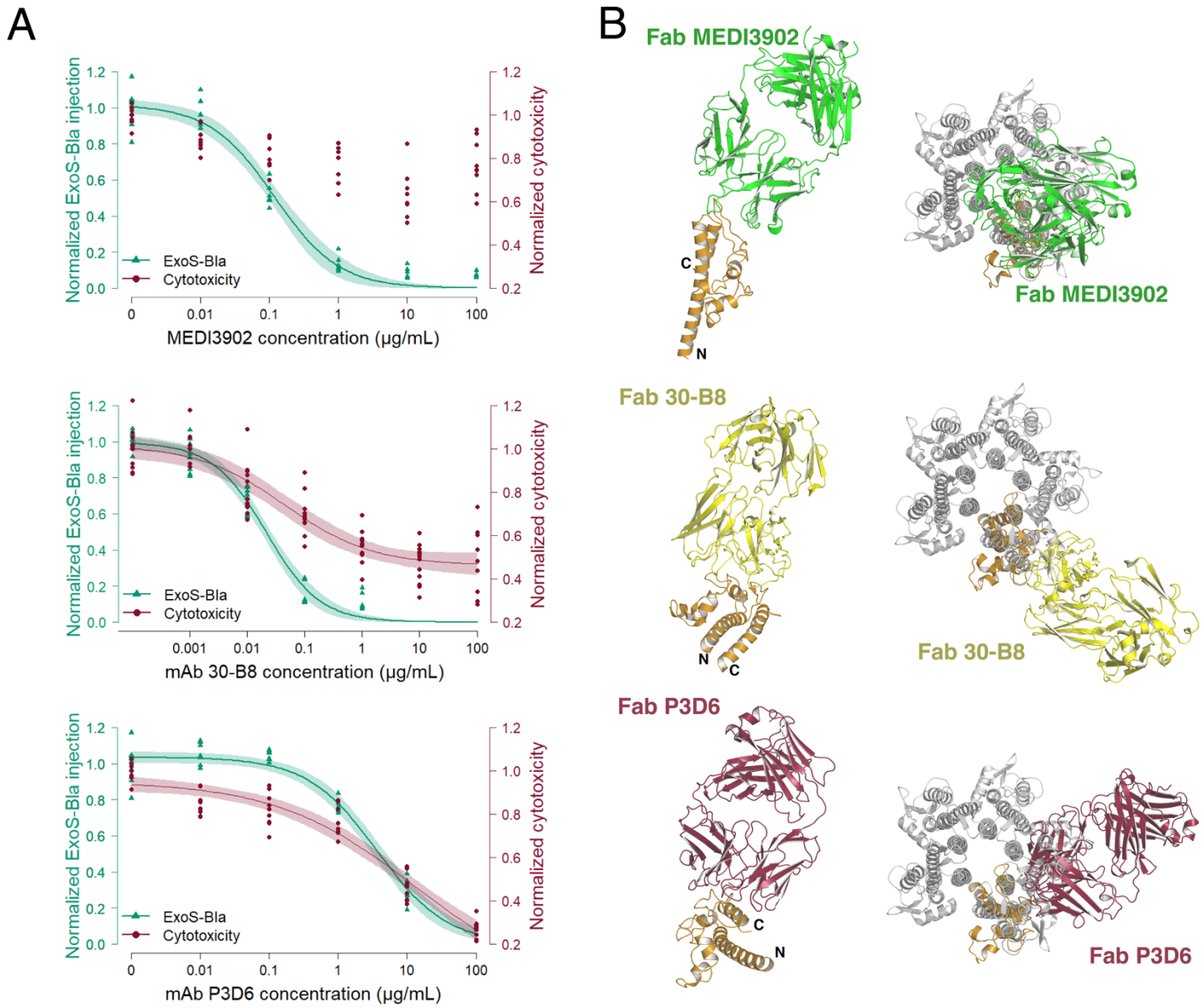

Figure 6. Functional and structural comparisons between anti-PcrV mAbs.

(A) Dose-dependent inhibition of T3SS in two functional assays reflecting toxin injection (ExoS-Bla injection) and translocon assembly (normalized J774 macrophage cytotoxicity) for three mAbs.

(B) Structures of PcrV-Fab complexes in the context of a PcrV monomer, as well as of a pentamer modeled based on the cryo-EM structure of SipD (Guo and Galan 2021). Fab P3D6 binds to a PcrV monomer but clashes with adjacent protomers in the context of the pentamer, while Fab MEDI3902 clashes with other Fab molecules. Fab 30-B8 binds to both the PcrV monomer and all pentamer protomers without clashes. N- and C- termini of PcrV are indicated in all structures, which are referenced in the main text.

AUTHOR CONTRIBUTIONS

JMD, EF, CCM, FC, LSDD, AA, IB, VTC and FC performed experiments and analyzed the data; EF, JMD, VTC, CCM and LSDD prepared the figures; DF and YC provided the tools and materials; IA, AD and PP designed the study, analyzed the data, and wrote the manuscript. All authors participated in discussions and editing of the final version of the manuscript.

DECLARATION OF INTERESTS

The authors declare no competing interests.

SUPPLEMENTARY DATA FOR

Neutralizing human monoclonal antibodies that target the PcrV component of the Type III Secretion System of *Pseudomonas aeruginosa* act through distinct mechanisms

Jean-Mathieu Desveaux[1], Eric Faudry[1], Carlos Contreras-Martel[1], François Cretin[1], Leonardo Sebastian Dergan-Dylon[1], Axelle Amen[1,2], Isabelle Bally[1], Victor Tardivy-Casemajor[1], Fabien Chenavier[1], Delphine Fouquenet[3], Yvan Caspar[1,4], Ina Attrée*[1], Andréa Dessen*[1], Pascal Poignard*[1,5]

[1] Univ. Grenoble Alpes, CEA, CNRS, Institut de Biologie Structurale (IBS), F-38044 Grenoble, France

[2] Laboratoire d'Immunologie, CHU Grenoble Alpes, France

[3] Centre d'Étude des Pathologies Respiratoires INSERM U1100 UFR de Médecine de Tours, 10 Bd Tonnellé, 37032 Tours Cedex

[4] Laboratoire de Bactériologie-Hygiène Hospitalière, CHU Grenoble Alpes, France

[5] Laboratoire de Virologie, CHU Grenoble Alpes, France

Supplementary Table 1. Sequence conservation of V and J regions of selected mAbs compared to germline. Percentage (%) of identity was obtained by aligning variable region sequences on IMGT database (https://www.imgt.org).

Anti-PcrV mAbs

Heavy chain	V Gene and allele	J Gene and allele	V region identity (%)	J region identity (%)	CDR3 length	Donor #
P3G9Hc	IGHV4-61*08	IGHJ6*02	92.44	91.94	18	16
P3D6Hc	IGHV3-23*01	IGHJ4*02	92.70	89.58	14	25
P5B3Hc	IGHV3-74*01	IGHJ3*02	96.88	94.00	11	25
P5E10Hc	IGHV3-21*01	IGHJ6*02	88.42	74.20	12	25
Light chain	**V Gene and allele**	**J Gene and allele**	**V region identity (%)**	**J region identity (%)**	**CDR3 length**	**Donor #**
P3G9κc	IGKV3-20*01	IGKJ3*01	94.68	100.00	10	16
P3D6κc	IGKV1-8*01	IGKJ4*01	96.41	97.37	9	25
P5B3λc	IGLV3-25*03	IGLJ2*01	96.10	100.00	11	25
P5E10κc	IGKV4-1*01	IGKJ4*01	95.00	100.00	9	25

Anti-PscF mAbs

Heavy chain	V Gene and allele	J Gene and allele	V region identity (%)	J region identity (%)	CDR3 length	Donor #
P1B7Hc	IGHV3-23*01	IGHJ4*02	97.22	91.67	13	25
P1D5Hc	IGHV4-61*02	IGHJ6*02	83.85	80.65	19	25
P1B4Hc	IGHV3-23*01	IGHJ6*02	95.14	83.87	17	25
P1F5Hc	IGHV3-23*01	IGHJ6*02	77.86	83.87	19	25
P1D7Hc	IGHV3-23*01	IGHJ4*02	96.87	93.75	15	25
P3G2Hc	IGHV4-61*02	IGHJ4*02	91.40	93.75	16	25
P3G6Hc	IGHV3-23*01	IGHJ6*02	98.61	85.48	17	25
P3G7Hc	IGHV3-72*01	IGHJ3*01	86.39	88.00	18	25
P5D5Hc	IGHV3-23*01	IGHJ4*02	96.52	93.75	13	25
P5G10Hc	IGHV4-34*01	IGHJ6*02	91.22	77.42	16	25
Light chain	**V Gene and allele**	**J Gene and allele**	**V region identity (%)**	**J region identity (%)**	**CDR3 length**	**Donor #**
P1B7κc	IGKV1-16*02	IGKJ2*01	97.13	97.14	9	25
P1D5κc	IGKV2-28*01	IGKJ3*01	94.22	100.00	9	25
P1B4κc	IGKV3-20*01	IGKJ1*01	95.04	97.14	9	25
P1F5κc	IGKV2-28*01	IGKJ2*01	95.58	89.47	17	25
P1D7λc	IGLV3-21*02	IGLJ2*01	98.56	97.37	11	25
P3G2λc	IGLV2-8*01	IGLJ2*01	94.79	88.57	10	25
P3G6κc	IGKV3-20*01	IGKJ2*01	99.60	89.74	9	25
P3G7λc	IGLV1-51*01	IGLJ2*01	88.00	91.67	11	25
P5D5κc	IGKV1-16*01	IGKJ2*01	98.20	94.29	9	25
P5G10λc	IGLV1-47*01	IGLJ2*01	94.73	91.67	11	25

Supplementary Table 2. Competition between A) anti-PscF mAbs and B) anti-PscF mAbs. The indicated IC_{50} values correspond to the concentration of competitor mAbs necessary to obtain half of the signal generated by the biotinylated mAbs without competitor. ND corresponds to a non-detectable competition.

Competitor mAbs	Detection mAbs: P1D8*	P1B7*	P5D5*	P3G6*	P5G10*	P1D6*	P1B4*	P1D5*
P1D8	0.01	ND	ND	ND	ND	ND	ND	ND
P1B7	ND	0.19	0.16	0.16	ND	0.60	0.20	0.52
P5D5	ND	0.39	0.68	0.46	ND	0.33	0.26	1.39
P3G6	ND	12.66	2.99	1.77	ND	8.37	5.18	7.99
P5G10	ND	ND	ND	ND	0.46	ND	ND	ND
P1D6	ND	15.02	0.89	1.17	ND	1.62	1.83	5.30
P1B4	ND	2.83	0.61	2.06	ND	7.67	1.97	5.00
P1D5	ND	14.21	0.86	0.70	ND	3.85	0.23	0.69

IC_{50} (µg/mL)
ND
9-20
4-8
<3

Competitor mAbs	Detection mAbs: P3G9*	P3D6*	P5B3*	P5E10*
P3G9	0.98	ND	ND	ND
P3D6	ND	0.80	0.28	ND
P5B3	ND	2.42	0.41	ND
P5E10	ND	ND	ND	0.51

IC_{50} (µg/mL)
ND
9-20
4-8
<3

Supplementary Table 3. Affinities of anti-PcrV mAbs for PcrV. The reported values correspond to the average of the measurements obtained from two independent experiments (n=2). Standard Deviations were calculated by the BLI analysis software.

IgG/His-PcrV-avitag	K_D (10^{-12}M)	K_{on} (10^2/Ms)	k_{on2} (1/Ms)	K_{off} (10^{-7}/s)	k_{off2} (10^{-3}/s)	R^2
P5B3	23.9 ± n.d	362 ± 38.2	1.2 ± 0.2	9.3 ± n.d	321.15 ± 49.7	0.9998
P3D6	736.8 ± 19	618 ± 1.5	0.4 ± 0.2	463.5 ± 12,7	12.3 ± 5.9	0.9997

Supplementary Table 4. Data collection, phasing and structure refinement statistics

DATA COLLECTION

X-ray source (Beamline)	ESRF (ID30A-1)
Detector	Pilatus 2M
Wavelength (Å)	0.965459
Scan-range (°)	180
Oscillation (°)	0.2
Space group	$P2_1$
a (Å)	87.58
b (Å)	87.58
c (Å)	105.22
α (°)	90.00
β (°)	104.83
γ (°)	90.00
Mosaicity (°)	0.129
Overall resolution (Å)	49.21-2.56
No. observed/unique reflections	176390/52157
High resolution shell (Å)	2.71-2.56
Completeness (%) (last shell)	99.5(99.2)
R_{sym} (%) (last shell)	21.7 (152.9)
$I/\sigma(I)$ (last shell)	5.02 (0.72)
$CC_{1/2}$	97.7 (31.2)
Wilson plot B-factor (Å^2)	45.86
MOLECULAR REPLACEMENT	
Phaser LLG	1032.93
R_{work}/R_{free} (%)	35.68/40.33
REFINEMENT	
Initial R_{work}/R_{free} (%)	35.68/40.33
Final R_{work}/R_{free} (%)	19.69/23.64
Final+TLS R_{work}/R_{free} (%)	20.97/23.70
STEREOCHEMICAL QUALITY	
RMS deviation, bond lengths (Å)	0.006
RMS deviation, bond angles (º)	1.266
Mean B-factor (Å^2)	46.74
No. of atoms	9052
No. of protein atoms	8614
No. of water molecules	392
Residues in most favored/allowed region of Ramachandran plot (%)	99.80

Supplementary Table 5. Bacterial strains and plasmids

***P. aeruginosa* strains**	**Characteristics**	**Reference or source**
CHAΔ*exoS*::*exoS-bla*	β-lactamase (bla) reporter for ExoS translocation	Verove et al., 2012
CHAΔ*pcrV*	Strain lacking *pcrV*	Gouré et al., 2004
PAO1Δ3Tox	Strain lacking toxins ExoS, ExoT and ExoY	Cisz et al., 2008
Plasmids	**Characteristics**	**Reference or source**
pIApG-*pcrV*-V1 (PAO1)	Replicative plasmid for PcrV expression, *$Leu^{6}Ala^{9}Ser^{21}Ser^{225}$	Lab collection; Simona Barzu, Lyon
pIApG-*pcrV*-V2 (CHA)	$Leu^{6}Ala^{9}Ser^{21}Arg^{225}$	Lab collection; Simona Barzu, Lyon
pIApG-*pcrV*-V3 (PA14)	$Phe^{6}Ala^{9}Pro^{21}Lys^{225}$	Lab collection; Simona Barzu, Lyon
pIApG-*pcrV*-V4 (PA103)	$Phe^{6}Gly^{9}Pro^{21}Arg^{225}$	Lab collection; Simona Barzu, Lyon
pIApG-*pcrV*-V5	$Phe^{6}Gly^{9}Pro^{21}Lys^{225}$	Lab collection; Simona Barzu, Lyon
pET15b-His-PcrV	Replicative plasmid for inducible His-PcrV expression	Nanao et al., 2003
pET22b-PscF-His	Replicative plasmid for inducible PscF-His expression	Quinaud et al, 2005
pESPRIT-His-PcrV-avitag	Replicative plasmid for inducible His-PcrV-avitag expression expression	This study
pESPRIT-His-PscF-avitag	Replicative plasmid for inducible expression His-PscF-avitag	This study

*variable residues within PcrV

Supplementary Figure 1. Dose-dependent inhibition by mAbs P5B3 and P3D6 of ExoS-Bla injection from strains expressing five PcrV variants. Inhibition of ExoS-Bla activity following infection of A495 epithelial cells with *P. aeruginosa* expressing the V1 (A and B), V2 (C), V3 (D), V4 (E) or V5 (F) variants, with mAbs concentration ranging from 0.01 to 100 µg/mL. (A and B) Both mAbs P5B3 (A) and P3D6 (B) display dose-response inhibition with the strain expressing the V1 variant, with respective IC_{50} of 96 and 3.7 µg/mL. (C to F) Monoclonal Ab P5B3 displays dose-response inhibition with the strain expressing the V2, V3, V4 and V5 variants with respective IC50 of 206, 192, 212 and 426 µg/mL. P3D6 had no effect on strains expressing variants 2, 3, 4 and 5 (see Fig. 3B).

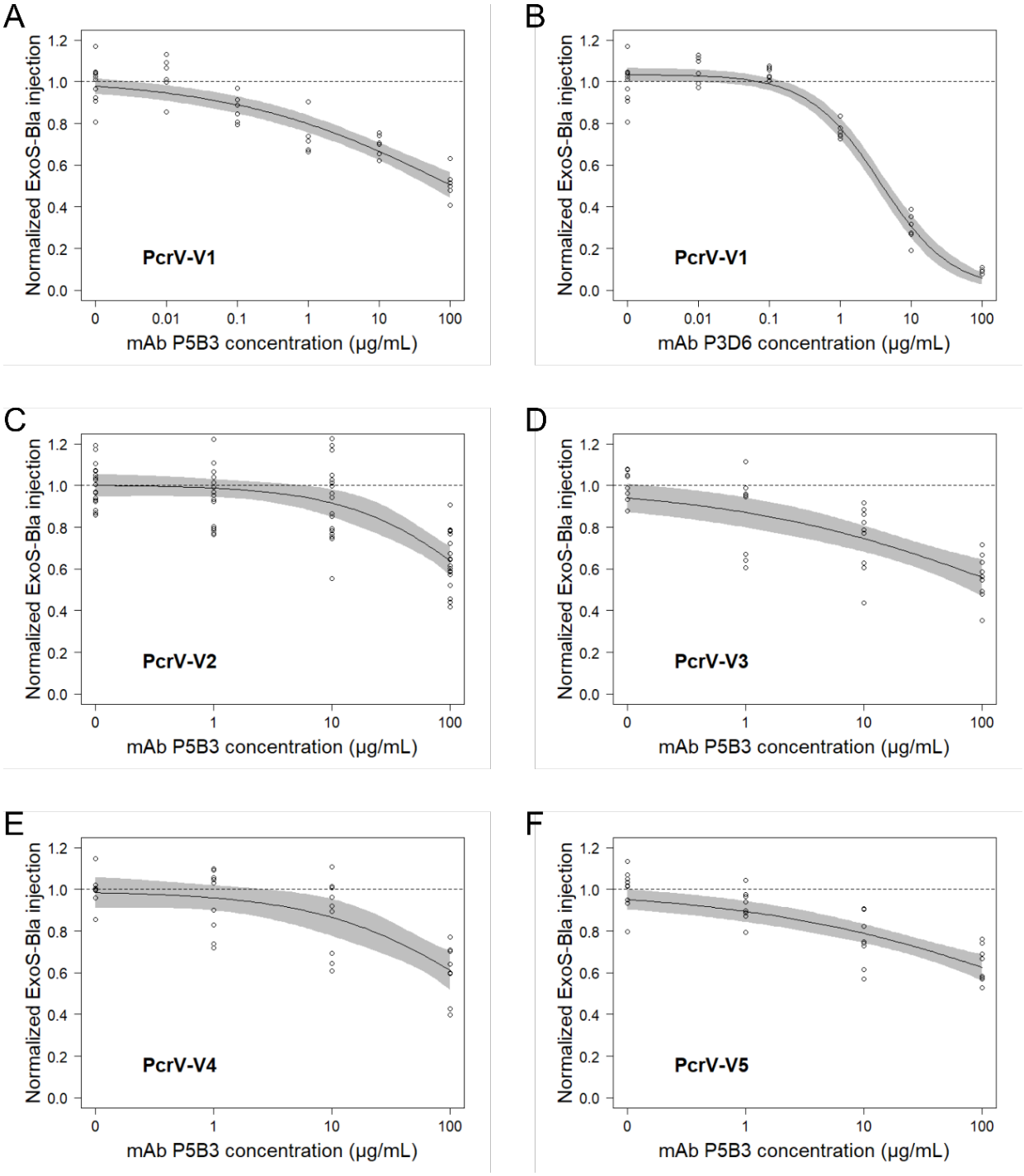

Supplementary Figure 2. Dose-dependent inhibition by mAbs 30-B8 of ExoS-Bla injection from strains expressing five PcrV variants. Inhibition of ExoS-Bla activity following infection of A495 epithelial cells with *P. aeruginosa* expressing the V1, V2, V3, V4 or V5 variants, with mAbs concentration ranging from 0.001 to 1 µg/mL. Monoclonal Ab 30-B8 displays dose-response inhibition with V1, V2, V3, V4 and V5 variants with respective IC50 of 21.3, 12.8, 11.2, 13.0, 10.5 ng/mL.

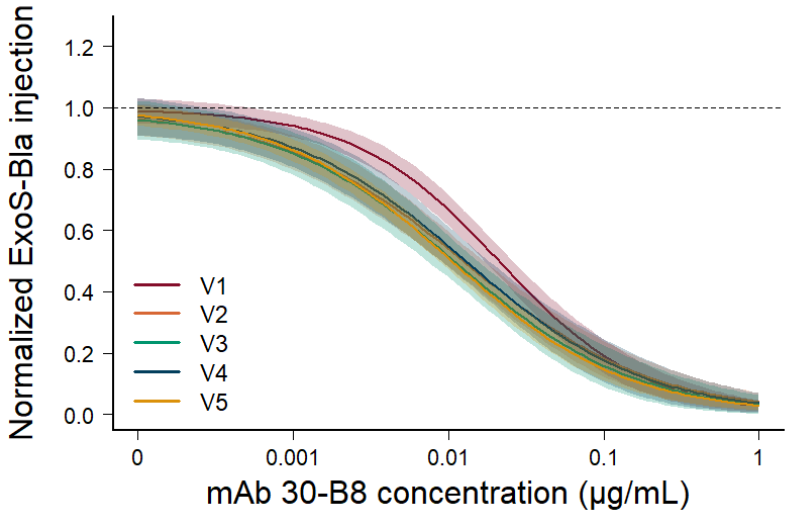

SUPPLEMENTARY REFERENCES

Cisz M, Lee P-C, Rietsch A. 2008. ExoS Controls the Cell Contact-Mediated Switch to Effector Secretion in *Pseudomonas aeruginosa*. *J Bacteriol* **190**:2726–2738. doi:10.1128/JB.01553-07

Goure J, Pastor A, Faudry E, Chabert J, Dessen A, Attree I. 2004. The V Antigen of *Pseudomonas aeruginosa* Is Required for Assembly of the Functional PopB/PopD Translocation Pore in Host Cell Membranes. *Infect Immun* **72**:4741–4750. doi:10.1128/IAI.72.8.4741-4750.2004

Nanao M, Ricard-Blum S, Di Guilmi A, Lemaire D, Lascoux D, Chabert J, Attree I, Dessen A. 2003. [No title found]. *BMC Microbiol* **3**:21. doi:10.1186/1471-2180-3-21

Quinaud M, Chabert J, Faudry E, Neumann E, Lemaire D, Pastor A, Elsen S, Dessen A, Attree I. 2005. The PscE-PscF-PscG Complex Controls Type III Secretion Needle Biogenesis in Pseudomonas aeruginosa. *Journal of Biological Chemistry* **280**:36293–36300. doi:10.1074/jbc.M508089200

Verove J, Bernarde C, Bohn Y-ST, Boulay F, Rabiet M-J, Attree I, Cretin F. 2012. Injection of Pseudomonas aeruginosa Exo Toxins into Host Cells Can Be Modulated by Host Factors at the Level of Translocon Assembly and/or Activity. *PLoS ONE* **7**:e30488. doi:10.1371/journal.pone.0030488